Weierstraß-Institut
für Angewandte Analysis und Stochastik

im Forschungsverbund Berlin e.V.

Preprint ISSN 0946 – 8633

Surface Diffusion of Graphs: Variational Formulation, Error Analysis and Simulation

Eberhard Bänsch[1], Pedro Morin[2] , Ricardo H. Nochetto[3]

submitted: December 20th 2002

[1] Weierstrass Institute for Applied Analysis and Stochastics, Mohrenstrasse 39, D - 10117 Berlin
and Freie Universität Berlin, Germany
email: baensch@wias-berlin.de

[2] Departamento de Matermática Facultad de Ingenieria Quimica, Universidad Nacional del Litoral
and Instituto de Matemática Aplicada del Litoral (IMAL), Güemes 3450, 3000 Santa Fe, Argentina
e-mail: pmorin@math.un1.edu.ar

[3] Department of Mathematics and Institute for Physical Science and Technology, University of Maryland
College Park, MD 20742, USA
e-mail: rhn@math.umd.edu

No. 797

Berlin 2002

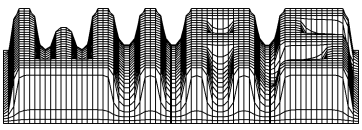

2000 *Mathematics Subject Classification.* 35K55, 65M12, 65M15, 65M60, 65Z05.

Key words and phrases. Surface diffusion, fourth-order parabolic problem, finite elements, a priori error estimates, Schur complement, smoothing effect.

Edited by
Weierstraß-Institut für Angewandte Analysis und Stochastik (WIAS)
Mohrenstraße 39
D — 10117 Berlin
Germany

Fax: + 49 30 2044975
E-Mail: preprint@wias-berlin.de
World Wide Web: http://www.wias-berlin.de/

SURFACE DIFFUSION OF GRAPHS: VARIATIONAL FORMULATION, ERROR ANALYSIS AND SIMULATION

EBERHARD BÄNSCH*, PEDRO MORIN†, AND RICARDO H. NOCHETTO‡

Abstract. Surface diffusion is a (4th order highly nonlinear) geometric driven motion of a surface with normal velocity proportional to the surface Laplacian of mean curvature. We present a novel variational formulation for graphs and derive a priori error estimates for a time-continuous finite element discretization. We also introduce a semi-implicit time discretization and a Schur complement approach to solve the resulting fully discrete, linear systems. After computational verification of the orders of convergence for polynomial degrees 1 and 2, we show several simulations in 1d and 2d with and without forcing which explore the smoothing effect of surface diffusion as well as the onset of singularities in finite time, such as infinite slopes and cracks.

Key words. Surface diffusion, fourth-order parabolic problem, finite elements, a priori error estimates, Schur complement, smoothing effect.

AMS subject classifications. 35K55, 65M12, 65M15, 65M60, 65Z05.

1. Introduction. Controlling morphological changes in stressed epitaxial films is of paramount importance in Materials Science. The film may be thought of as subjected to mechanical stresses to model its misfit with the crystalline structure of the substrate. This in turn causes a plastic deformation of the free surface of the film, a morphological instability of the free surface which may eventually lead to crack formation and fracture. The simplest model couples surface diffusion of the free surface with linear elasticity in the bulk [1, 7, 12, 13, 14, 17, 18, 19]. Investigating this complicated nonlinear dynamics requires effective and reliable computational tools.

This paper studies the *geometric* motion law of *surface diffusion* with given forcing, but without elasticity. The dynamics of the free surface $\Gamma(t)$ is thus governed by the (highly nonlinear) 4th order geometric PDE

$$V = -\Delta_S(\kappa + f), \tag{1.1}$$

where V is the normal velocity of $\Gamma(t)$, κ is its mean curvature, and Δ_S is the Laplace-Beltrami operator on $\Gamma(t)$. In this reduced model f is given, whereas in the full model f corresponds to the elastic energy density of the bulk $\Omega(t)$ restricted to $\Gamma(t)$. Our goal is to present novel variational formulations and finite element methods for (1.1), which may be viewed as building blocks towards solving the fully coupled system.

We study the *graph* case in this paper and the *parametric* case in [4]. From now on we assume that $\Omega \subseteq \mathbb{R}^d$ $(d \geq 1)$ is a fixed domain and $\Gamma(t) := \{(x, u(t,x)) \mid x \in \Omega\} \subseteq \mathbb{R}^{d+1}$ is the free surface for $0 \leq t \leq T$ described by the unknown function u. If $Q = Q(u) = \sqrt{1 + |\nabla u|^2}$ denotes the elementary surface area, then the unit normal

* Weierstrass Institute for Applied Analysis and Stochastics Mohrenstrasse 39, 10117 Berlin, and Freie Universität Berlin, GERMANY (baensch@wias-berlin.de).

† Instituto de Matemática Aplicada del Litoral (IMAL), Güemes 3450 and Departamento de Matemática, Facultad de Ingeniería Química, Universidad Nacional del Litoral, 3000 Santa Fe, Argentina (pmorin@math.unl.edu.ar). Partially supported by Programa FOMEC de la Universidad Nacional del Litoral and CONICET of Argentina and NSF Grant DMS-9971450. This work was partly developed while this author was visiting the University of Maryland.

‡ Department of Mathematics and Institute for Physical Science and Technology, University of Maryland, College Park, MD 20742, USA (rhn@math.umd.edu). Partially supported by NSF Grants DMS-9971450 and DMS-0204670.

ν to $\Gamma(t)$, its mean curvature κ, and the normal velocity V of $\Gamma(t)$ can be expressed as follows:

$$\nu = \frac{1}{Q}(-\nabla u, 1)^T, \qquad \kappa = \nabla \cdot \Big(\frac{\nabla u}{Q}\Big), \qquad V = \frac{\partial_t u}{Q}.$$

Therefore, (1.1) can be written as the following system of 2nd order nonlinear PDE

$$\frac{\partial_t u}{Q} = -\Delta_S(\kappa + f), \qquad \kappa = \nabla \cdot \Big(\frac{\nabla u}{Q}\Big), \tag{1.2}$$

for (u, κ). Once completed with initial and boundary conditions, this system constitutes our starting point.

We introduce in §2 a new variational formulation with several crucial stability properties. Using C^0 finite elements of any degree $k \geq 1$, we obtain a space discretization in §3 with solutions (u_h, κ_h), and show corresponding stability properties. After deriving a number of auxiliary results for the semidiscrete scheme in §4, we use them to prove the quasi-optimal estimate in §5 for the errors $e_u = u - u_h$ and $e_\kappa = \kappa - \kappa_h$:

$$\sup_{t\in[0,T]} \Big(\|e_u(t)\|_2^2 + \int_{\Gamma_h(t)} |\nabla_S e_u|^2\Big) + \int_0^T \Big(\|e_\kappa(t)\|_2^2 + \int_{\Gamma_h(t)} |\nabla_S e_\kappa|^2\Big)\, dt \leq C\, h^{2k}. \tag{1.3}$$

Here $C > 0$ depends on regularity of u and κ, $k \geq 1$ is the polynomial degree, and h is the meshsize. It is worth comparing our results with the existing literature. A space-time finite element method for *axially symmetric* surfaces is presented by Coleman et al in [8], along with several stability properties and very interesting dynamics, some not predicted by linearized stability. More recently, Deckelnick et al provided an error analysis [10] for the axially symmetric case. Our formulation, discretization, and analysis differ from those in [8, 10].

In §6 we introduce a *semi-implicit* time discretization in the spirit of Dziuk [9, 11]. This leads to a sequence of surfaces Γ^n and *linear* elliptic PDE on them. We derive again several crucial stability properties and discuss a Schur complement approach for doing effective numerical linear algebra. We finally show a number of numerical experiments in §7. Their purpose is twofold: first we computationally verify the rate (1.3) for $k = 1, 2$, and secondly we explore the nonlinear regime of (1.1) via simulation. In fact, we examine the regularizing effect of surface diffusion as well as whether (1.1) is capable of forming singularities. They manifest as vertical slopes $|\nabla u| = \infty$ for $f = 0$ and cracks for $f \neq 0$ of a special form. We display results for both $d = 1, 2$ computed with the finite element toolbox ALBERT [16, 15].

2. Variational Formulation. In this section we write (1.2) in weak form. We start with some notation and basic formulas.

2.1. Elementary Differential Geometry. Let $v, w : \Omega \to \mathbb{R}$ be (smooth) functions. Since the surface element is given by $Q\, dx$, then

$$\int_{\Gamma(t)} v = \int_\Omega v\, Q\, dx;$$

in particular, the area $A(t)$ of $\Gamma(t)$ reads $A(t) = \int_\Omega Q\, dx$ at time t. If $\tilde{v}$ is the trivial extension of v to $\mathbb{R}^{d+1}$, namely, $\tilde{v}(x_1, \ldots, x_{d+1}) := v(x_1, \ldots, x_d)$, then the *tangential* gradient ∇_S is given by

$$\nabla_S v = \nabla_{d+1}\tilde{v} - \nabla_{d+1}\tilde{v} \cdot \nu\, \nu,$$

where ∇_{d+1} denotes the gradient in $\mathbb{R}^{d+1}$. Since $\nabla_{d+1}\tilde{v} = (\nabla v^T, 0)^T$, we readily get

$$\nabla_S v \cdot \nabla_S w = \nabla v \cdot \nabla w - \frac{1}{Q^2} \nabla v \cdot \nabla u \; \nabla w \cdot \nabla u.$$

Note that there is also an intrinsic definition of ∇_S. If $\gamma = \partial\Gamma$ indicates the boundary of Γ, then this expression, together with integration by parts, yields

$$\begin{aligned} -\int_\Gamma \Delta_S v \, w + \int_\gamma \underline{\partial}_{\nu_\gamma} v \, w \, d\mathcal{H}^{d-2} &= \int_\Gamma \nabla_S v \cdot \nabla_S w = \int_\Omega \nabla_S v \cdot \nabla_S w \, Q \, dx \\ &= \int_\Omega \Big(\nabla v \cdot \nabla w \, Q - \frac{\nabla v \cdot \nabla u \, \nabla w \cdot \nabla u}{Q} \Big) \, dx. \end{aligned} \tag{2.1}$$

Here ν_γ denotes the intrinsic outer unit normal of Γ at γ, given by $\nu_\gamma = \nu_\Gamma \wedge \tau_\gamma$ with τ_γ the tangential unit vector of γ with appropriate sign for $\Gamma \subseteq \mathbb{R}^3$.

2.2. Boundary Conditions and Function Spaces. Let $L^p(\Omega)$, $1 \le p \le \infty$ be the usual space of Lebesgue measurable functions with norm $\|v\|_p := (\int_\Omega |v(x)|^p dx)^{1/p}$. By $\langle \cdot, \cdot \rangle$ we denote the L^2 inner product $\langle v, w \rangle := \int_\Omega v(x) w(x) \, dx$ for $v, w \in L^2(\Omega)$. We indicate with $H^{m,p}(\Omega)$ the Sobolev space of functions in $L^p(\Omega)$ with m–th weak derivatives also in $L^p(\Omega)$ equipped with the norm $\|v\|_{m,p} := \big(\sum_{|\alpha| \le m} \int_\Omega |\partial_\alpha v|^p \big)^{1/p}$ and $H^m := H^{m,2}$. Furthermore, $\mathring{H}^1(\Omega)^p$ is the subspace of functions in $H^{1,p}$ with vanishing boundary values in the sense of traces.

Finally, for a time interval $[0, T]$ and a function space V we define the parabolic spaces $L^p(V)$ of V-valued functions that are measurable in time with $\|v\|_{L^p(V)} := (\int_0^T \|v(t)\|_V dt)^{1/p} < \infty$.

To simplify the notation we will write $\|v\|_\infty = \|v\|_{L^\infty(L^\infty)}$. This ambiguity of notation will not lead to confusion.

We now discuss boundary conditions and corresponding function spaces $\mathcal{X}$.

Periodic boundary condition: Let $\Omega = \Pi_{i=1}^d (0, X_i)$ be a parallelogram. If $u(t, x + X_i e_i) = u(t, x), \kappa(t, x + X_i e_i) = \kappa(t, x)$ for all $x \in \partial\Omega$ and $1 \le i \le d$, then

$$\mathcal{X} := \{ v \in H^1(\Omega) \mid v(t, x + X_i e_i) = v(t, x) \quad \text{for } x \in \partial\Omega, \; 1 \le i \le d \}.$$

Neumann boundary condition: If $\nu_\gamma \cdot \nabla_S u(t, x) = \nu_\gamma \cdot \nabla_S \kappa(t, x) = 0$ for $x \in \partial\Omega$, then $\mathcal{X} := H^1(\Omega)$.

Dirichlet Boundary Condition: If $u(t, x) = \kappa(t, x) = 0$ for $x \in \partial\Omega$, then $\mathcal{X} := \mathring{H}^1(\Omega)$.

2.3. Weak Form. We are now in the position to introduce two bilinear forms in (v, w) and state the variational formulation of (1.2). Let

$$\boldsymbol{a}(u; v, w) := \int_\Omega \big(\nabla v \cdot \nabla w \, Q - \frac{\nabla v \cdot \nabla u \, \nabla w \cdot \nabla u}{Q} \big) \, dx, \tag{2.2}$$

$$\tilde{\boldsymbol{a}}(u; v, w) := \int_\Omega \frac{\nabla v \cdot \nabla w}{Q} \, dx. \tag{2.3}$$

LEMMA 2.1 (Equivalence). *Let $u \in C^1([0, T]; C^4(\bar{\Omega}))$, $\kappa \in C^0([0, T]; C^2(\bar{\Omega}))$ and let $\mathcal{X}$ be as defined in §2.2. Then (u, κ) is a solution of (1.2) with initial value u_0 and boundary conditions as in §2.2 iff $u(t)$,$\kappa(t) \in \mathcal{X}$ for all $t \in [0, T]$, $u(0, \cdot) = u_0$, and*

$$\langle \partial_t u, \psi \rangle - \boldsymbol{a}(u; \kappa, \psi) = \boldsymbol{a}(u; f, \psi) \qquad \forall \; \psi \in \mathcal{X}, \tag{2.4}$$

$$\langle \kappa, \varphi \rangle + \tilde{\boldsymbol{a}}(u; u, \varphi) = 0 \qquad \forall \; \varphi \in \mathcal{X}. \tag{2.5}$$

Proof. Multiply the first equation in (1.2) by ψ, integrate over Γ and use formula (2.1). Observe that the boundary term vanishes because of the choice of function space $\mathcal{X}$. Equation (2.5) follows similarly from the second equation in (1.2) integrating by parts over Ω. ∎

REMARK 2.2 (Mean Curvature Flow). In contrast to the mean curvature flow, for which a divergence formulation reads [9, 11]

$$\int_\Omega \frac{\partial_t u\, v}{Q}\, dx + \tilde{\boldsymbol{a}}(u;u,v) = 0 \qquad \forall\ v \in \mathcal{X},$$

we do not have the factor $\frac{1}{Q}$ in the parabolic term.

REMARK 2.3 (Comparing $\boldsymbol{a}$ and $\tilde{\boldsymbol{a}}$). The forms $\boldsymbol{a}$ and $\tilde{\boldsymbol{a}}$ are symmetric and non-negative. If $d = 1$, they coincide $\boldsymbol{a}(u;\cdot,\cdot) = \tilde{\boldsymbol{a}}(u;\cdot,\cdot)$. If $d > 1$, instead,

$$\boldsymbol{a}(u;v,u) = \tilde{\boldsymbol{a}}(u;v,u) \qquad \forall\ v \in \mathcal{X}$$

because $Q(1 - \frac{|\nabla u|^2}{Q^2}) = \frac{1}{Q}$. Similarly

$$\boldsymbol{a}(u;v,v) = \int_\Gamma \nabla_S v \cdot \nabla_S v = \int_\Omega \Big(|\nabla v|^2 Q - \frac{|\nabla v \cdot \nabla u|^2}{Q}\Big)\, dx \geq \int_\Omega \frac{|\nabla v|^2}{Q}\, dx = \tilde{\boldsymbol{a}}(u;v,v).$$

REMARK 2.4 (Equivalent Forms of $\boldsymbol{a}$). Let $\zeta := \frac{\nabla u}{|\nabla u|}$ be a unit vector in the direction of ∇u provided $\nabla u \neq 0$ and arbitrary otherwise. Let $(\chi_i)_{i=1}^{d-1}$ be a complementary orthonormal set perpendicular to ζ. A simple calculation then yields

$$\boldsymbol{a}(u;v,w) = \int_\Omega \Big(\frac{\nabla v\cdot\zeta\, \nabla w\cdot\zeta}{Q} + Q\sum_{i=1}^{d-1} \nabla v\cdot\chi_i\, \nabla w\cdot\chi_i\Big) dx \qquad \forall\ v,w \in \mathcal{X}. \tag{2.6}$$

Another equivalent form is obtained using $\otimes$ to denote the tensor product in $\mathbb{R}^d$:

$$\boldsymbol{a}(u;v,w) = \int_\Omega \nabla v^T \left(Q\, I - \frac{\nabla u \otimes \nabla u}{Q}\right) \nabla w\, dx, \tag{2.7}$$

here I denotes the identity matrix in $\mathbb{R}^d$.

REMARK 2.5 (Volume Conservation and Area Decrease). If the function $v = 1 \in \mathcal{X}$, then (2.4) yields $0 = \langle \partial_t u, 1\rangle = \partial_t \int_\Omega u\, dx$, which is the formula for conservation of volume. On the other hand, if the forcing term $f \equiv 0$, then the area of $\Gamma(t)$ is decreasing regardless of boundary conditions (see Lemma 2.6). Both of these properties will also hold true for the semi-discrete and fully discrete formulations of §3 and §6.

With the help of the above variational form of the equations, we are in a position to prove a stability result for the continuous solution.

LEMMA 2.6 (Continuous Stability). *Let (u,κ) be a solution of (1.2) fulfilling the assumptions of Lemma 2.1, and let $A(t)$ denote the area of $\Gamma(t)$. There are two constants $C_1 = C_1(\Omega)$ and $C_2 = C_2\big(\|\nabla f\|_\infty, A(0)\big)$, such that*

$$\sup_{t\in[0,T]} \|u(t)\|_2^2 + \int_0^T \|\kappa\|_2^2\, dt \leq \|u(0)\|_2^2 + C_1 \int_0^T \|\nabla f(t)\|_2\, dt,$$

$$\sup_{t\in[0,T]} A(t) + \int_0^T \boldsymbol{a}(u;\kappa,\kappa)\, dt \leq C_2.$$

Moreover, if $f \equiv 0$, then the function $A(t)$ is decreasing (strictly provided $\Delta_S \kappa \not\equiv 0$).

Proof. We omit the proof because it is the same as that of Proposition 3.2. ∎

3. Space Discretization. Let $(\mathcal{T}_h)_{h>0}$ be a family of (possibly graded) shape regular triangulations of Ω with h being the largest size of elements in $\mathcal{T}_h$. We fix $k \in \mathbb{N}$ and denote by $\mathcal{X}_h \subseteq \mathcal{X}$ the subspace of continuous finite elements of polynomial degree k with appropriate boundary conditions. Let $I_h : \mathcal{X} \cap C^0(\bar{\Omega}) \to \mathcal{X}_h$ be an interpolation operator fulfilling

$$\|I_h v - v\|_p + h\|\nabla(I_h - v)\|_p \le C\, h^{k+1}\|v\|_{k+1,p} \tag{3.1}$$

for $1 \le p \le \infty$ and $v \in H^{k+1,p}(\Omega)$ [6]. We will not need an inverse estimate for the error analysis and thus we do not require quasi-uniformity of the underlying meshes.

DEFINITION 3.1 (Semidiscrete Solution). *A pair u_h, κ_h with $u_h \in C^1([0,T], \mathcal{X}_h)$, $\kappa_h \in C^0([0,T]; \mathcal{X}_h)$ is called a* semidiscrete solution *of (1.2) if $u_h(0,\cdot) = I_h u_0$ and*

$$\langle \partial_t u_h, \psi_h\rangle - \boldsymbol{a}(u_h; \kappa_h, \psi_h) = \boldsymbol{a}(u_h; f, \psi_h) \qquad \forall\ \psi_h \in \mathcal{X}_h, \tag{3.2}$$

$$\langle \kappa_h, \varphi_h\rangle + \tilde{\boldsymbol{a}}(u_h; u_h, \varphi_h) = 0 \qquad \forall\ \varphi_h \in \mathcal{X}_h. \tag{3.3}$$

From now on we consider $d \ge 2$, the analysis for $d = 1$ is just a simplified version of this case. We recall from Remark 2.4 that $\{\zeta, \chi_1, \dots, \chi_{d-1}\}$ is a set of orthonormal vectors for which (2.6) holds. If $\{\zeta_h, \chi_{h,1}, \dots, \chi_{h,d-1}\}$ denotes likewise a semidiscrete orthonormal set, and $Q_h = Q(u_h)$, then

$$\boldsymbol{a}(u_h; v, w) = \int_\Omega \Big(\frac{\nabla v\cdot\zeta_h\, \nabla w\cdot\zeta_h}{Q_h} + \sum_{i=1}^{d-1} \nabla v\cdot\chi_{h,i}\, \nabla w\cdot\chi_{h,i}\, Q_h \Big)\, dx \tag{3.4}$$

PROPOSITION 3.2 (Semidiscrete Stability). *Let (u_h, κ_h) be a semidiscrete solution in the sense of Definition 3.1, and let $A_h(t) := \int_\Omega Q_h\, dx$ denote the area of the surface $\Gamma_h(t) := \{(x, u_h(t,x)) \mid x \in \Omega\}$. There are two constants $C_1 = C_1(\Omega)$ and $C_2 = C_2\big(\|\nabla f\|_\infty, A_h(0)\big)$, such that*

$$\sup_{t\in[0,T]} \|u_h(t)\|_2^2 + \int_0^T \|\kappa_h\|_2^2\, dt \le \|u_h(0)\|_2^2 + C_1 \int_0^T \|\nabla f(t)\|_2\, dt. \tag{3.5}$$

$$\sup_{t\in[0,T]} A_h(t) + \int_0^T \boldsymbol{a}(u_h; \kappa_h, \kappa_h)\, dt \le C_2 \tag{3.6}$$

Moreover, if $f \equiv 0$, the function $A_h(t)$ is decreasing (strictly if $\boldsymbol{a}(u_h; \kappa_h, \kappa_h) > 0$).

Proof. First choose $\psi_h := u_h$, $\varphi_h := \kappa_h$ as test functions in (3.2) and (3.3), respectively. In view of Remark 2.3, we get

$$\langle \partial_t u_h, u_h\rangle + \langle \kappa_h, \kappa_h\rangle + \underbrace{\tilde{\boldsymbol{a}}(u_h; u_h, \kappa_h) - \boldsymbol{a}(u_h; \kappa_h, u_h)}_{=0} = \boldsymbol{a}(u_h; f, u_h).$$

and, since $|\nabla u_h|/Q_h \le 1$,

$$\boldsymbol{a}(u_h; f, u_h) = \tilde{\boldsymbol{a}}(u_h; f, u_h) = \int_\Omega \frac{\nabla f\cdot\nabla u_h}{Q_h} dx \le \|\nabla f\|_2 \Big(\int_\Omega \frac{|\nabla u_h|^2}{Q_h^2} \Big)^{1/2} dx \le C_1 \|\nabla f\|_2.$$

Integrating in time gives (3.5). We next set $\psi_h := -\kappa_h$, $\varphi_h := \partial_t u_h$ to derive

$$\underbrace{-\langle \partial_t u_h, \kappa_h\rangle + \langle \kappa_h, \partial_t u_h\rangle}_{=0} + \boldsymbol{a}(u_h; \kappa_h, \kappa_h) + \tilde{\boldsymbol{a}}(u_h; u_h, \partial_t u_h) = -\boldsymbol{a}(u_h; f, \kappa_h).$$

Observing that

$$\tilde{\boldsymbol{a}}(u_h; u_h, \partial_t u_h) = \int_\Omega \frac{\nabla u_h \cdot \nabla \partial_t u_h}{Q_h} = \partial_t \int_\Omega Q_h = \partial_t A_h(t) \tag{3.7}$$

we get

$$\partial_t A_h(t) + \boldsymbol{a}(u_h; \kappa_h, \kappa_h) = -\boldsymbol{a}(u_h; f, \kappa_h).$$

which implies that $A_h(t)$ is decreasing provided $f \equiv 0$. To prove (3.6) for $f \not\equiv 0$, we have to bound $\boldsymbol{a}(u_h; f, \kappa_h)$. Making use of (3.4), we obtain

$$\begin{aligned}
\boldsymbol{a}(u_h; f, \kappa_h) &= \int_\Omega \Big(\frac{\nabla f \cdot \zeta_h \, \nabla \kappa_h \cdot \zeta_h}{Q_h} + \sum_{i=1}^{d-1} \nabla f \cdot \chi_{h,i} \, \nabla \kappa_h \cdot \chi_{h,i} \, Q_h \Big) \, dx \\
&\le \|\nabla f\|_\infty \int_\Omega \Big(\frac{|\nabla \kappa_h \cdot \zeta_h|}{Q_h} + \sum_{i=1}^{d-1} |\nabla \kappa_h \cdot \chi_{h,i}| \, Q_h \Big) \, dx \\
&\le \|\nabla f\|_\infty \Big(\frac{|\Omega|}{4\epsilon} + \epsilon \int_\Omega \Big(\frac{|\nabla \kappa_h \cdot \zeta_h|^2}{Q_h} + \sum_{i=1}^{d-1} |\nabla \kappa_h \cdot \chi_{h,i}|^2 Q_h \Big) dx + \frac{\int_\Omega Q_h dx}{4\epsilon} \Big) \\
&= \|\nabla f\|_\infty \Big(C_\epsilon + \epsilon \, \boldsymbol{a}(u_h; \kappa_h, \kappa_h) + C_\epsilon A_h(t) \Big),
\end{aligned}$$

where we have used that $Q_h \ge 1$. Choosing ϵ sufficiently small, a Gronwall argument finally yields (3.6). ∎

COROLLARY 3.3 (Global Existence of Semidiscrete Solution). *For $h > 0$ and $T > 0$ there is a unique semidiscrete solution (u_h, κ_h) fulfilling (3.2) and (3.3).*

Proof. Observing that (3.2)–(3.3) is equivalent to a system of ordinary differential equations with a locally Lipschitz right hand side we get a local in time existence of the semi discrete solution. Using the above stability estimate, this solution can be extended to the time interval $[0, T]$ by standard arguments. Uniqueness follows from the local Lipschitz continuity of the right hand side. ∎

4. Auxiliary Estimates. In this section we present some auxiliary lemmas and results that will be instrumental in deriving the error estimates. Since they will be used several times and might be of independent interest, we present them separately.

We start introducing the following notation:

$$e_u := u - u_h, \qquad e_\kappa := \kappa - \kappa_h, \qquad N_h := \int_\Omega |\nu - \nu_h|^2 Q_h \, dx.$$

LEMMA 4.1 (Basic Geometric Formulas). *Using the notation introduced above, the following inequalities hold*

$$|\frac{1}{Q} - \frac{1}{Q_h}| \le |\nu - \nu_h|, \qquad |Q - Q_h| \le Q Q_h |\nu - \nu_h|, \tag{4.1}$$

and

$$\left| \frac{\nabla u \otimes \nabla u}{Q} - \frac{\nabla u_h \otimes \nabla u_h}{Q_h} \right| \le 3 \, Q \, Q_h \, |\nu - \nu_h|. \tag{4.2}$$

Proof. Recalling that $\nu = \frac{1}{Q}(\nabla u, -1)^T$, and $\nu_h = \frac{1}{Q_h}(\nabla u_h, -1)^T$, the inequalities in (4.1) are immediate. To prove (4.2), let us introduce the notation $z := \frac{\nabla u}{Q}$ and $z_h := \frac{\nabla u_h}{Q_h}$, and observe that

$$\begin{aligned}\frac{\nabla u \otimes \nabla u}{Q} - \frac{\nabla u_h \otimes \nabla u_h}{Q_h} &= z \otimes z\, Q - z_h \otimes z_h\, Q_h \\ &= (z - z_h) \otimes z\, Q + z_h \otimes z\,(Q - Q_h) + z_h \otimes (z - z_h)\, Q_h.\end{aligned}$$

Therefore, the triangle inequality and the fact that $|z - z_h| \le |\nu - \nu_h|$ yield (4.2). ∎

The following lemma is crucial for our error analysis and provides a coercivity estimate for $\tilde{\boldsymbol{a}}$. The estimate is the same that appears in the error analysis for mean curvature flow, and is due to Deckelnick and Dziuk [9, 11]. Even though its proof can be found in [9, p. 347], we sketch it here for completeness.

LEMMA 4.2 (Coercivity of $\tilde{\boldsymbol{a}}$). *The following estimate holds true*

$$\tilde{\boldsymbol{a}}(u; u, \partial_t e_u) - \tilde{\boldsymbol{a}}(u_h; u_h, \partial_t e_u) \ge \frac{1}{2}\partial_t N_h(t) - \|\nabla \partial_t u(t)\|_\infty N_h(t).$$

Proof. We start with two geometric relations which follow by simple calculation:

$$1 - \frac{1 + \nabla u \cdot \nabla u_h}{Q Q_h} = \frac{1}{2}\big|\nu - \nu_h\big|^2, \quad \Big|\Big(\frac{1}{Q} - \frac{1}{Q_h}\Big)\Big(\frac{\nabla u}{Q} - \frac{\nabla u_h}{Q_h}\Big)\Big| \le \frac{1}{2}\big|\nu - \nu_h\big|^2. \quad (4.3)$$

We now use the first equality in (4.3) to realize that

$$\begin{aligned}\frac{1}{2}\partial_t\big(|\nu - \nu_h|^2 Q_h\big) &= \partial_t\Big(\big(1 - \frac{1 + \nabla u \cdot \nabla u_h}{Q Q_h}\big) Q_h\Big) \\ &= \frac{\nabla u_h \cdot \nabla \partial_t u_h}{Q_h} + \frac{\nabla u \cdot \nabla \partial_t u}{Q^3}\big(1 + \nabla u \cdot \nabla u_h\big) - \frac{1}{Q}\big(\nabla u_h \cdot \nabla \partial_t u + \nabla u \cdot \nabla \partial_t u_h\big),\end{aligned}$$

and upon adding and subtracting $\frac{\nabla u_h \cdot \partial_t \nabla u}{Q_h}$ and reordering terms, we find out that

$$\begin{aligned}\frac{1}{2}\partial_t\big(|\nu - \nu_h|^2 Q_h\big) = \Big(\frac{\nabla u}{Q} - \frac{\nabla u_h}{Q_h}\Big) \cdot \nabla \partial_t (u - u_h) \\ - \partial_t \nabla u \cdot \Big(\frac{\nabla u}{Q} - \frac{\nabla u_h}{Q_h} + \frac{\nabla u_h}{Q} - \frac{1 + \nabla u \cdot \nabla u_h}{Q^2}\frac{\nabla u}{Q}\Big).\end{aligned}$$

We next integrate over Ω, use the definition of N_h, and add and subtract $\nabla \partial_t u \cdot \nabla u \frac{Q_h}{Q^2}$ to obtain

$$\begin{aligned}\tilde{\boldsymbol{a}}(u; u, \partial_t e_u) - \tilde{\boldsymbol{a}}(u_h; u_h, \partial_t e_u) &= \int_\Omega \Big(\frac{\nabla u}{Q} - \frac{\nabla u_h}{Q_h}\Big) \cdot \nabla \partial_t (u - u_h)\, dx \\ &= \frac{1}{2}\partial_t \int_\Omega |\nu - \nu_h|^2 Q_h\, dx \\ &\quad + \int_\Omega \partial_t \nabla u \cdot \Big(\frac{\nabla u}{Q} - \frac{\nabla u_h}{Q_h}\Big)\Big(\frac{1}{Q_h} - \frac{1}{Q}\Big) Q_h\, dx \\ &\quad + \int_\Omega \partial_t \nabla u \cdot \frac{\nabla u}{Q^2}\Big(1 - \frac{1 + \nabla u \cdot \nabla u_h}{Q Q_h}\Big) Q_h\, dx \\ &\ge \frac{1}{2}\partial_t N_h(t) - \|\nabla \partial_t u(t)\|_\infty N_h(t),\end{aligned}$$

where we have employed both estimates (4.3). This finally concludes the proof. □

The following two lemmas are consistency estimates for the bilinear forms $\boldsymbol{a}$ and $\tilde{\boldsymbol{a}}$, respectively.

LEMMA 4.3 (Consistency estimate for $\boldsymbol{a}$). *For every $\epsilon > 0$ there exists a constant $C = C(\epsilon, \|\nabla\kappa\|_\infty, \|Q\|_\infty, \|\nabla f\|_\infty) > 0$ such that*

$$|\boldsymbol{a}(u;\kappa,w) - \boldsymbol{a}(u_h;\kappa_h,w)| \;\le\; \epsilon\,\boldsymbol{a}(u_h;e_\kappa,e_\kappa) \;+\; C\,\|\nabla w\|_\infty^2 \;+\; N_h(t), \qquad \forall w \in \mathcal{X}.$$

Proof. We first add and subtract the term $\boldsymbol{a}(u_h;\kappa,w)$ to obtain

$$\boldsymbol{a}(u;\kappa,w) - \boldsymbol{a}(u_h;\kappa_h,w) = \boldsymbol{a}(u_h;\kappa-\kappa_h,w) \;+\; \big(\boldsymbol{a}(u;\kappa,w) - \boldsymbol{a}(u_h;\kappa,w)\big) =: (I) \;+\; (II)$$

and analyze (I) and (II) separately. By Cauchy-Schwarz inequality,

$$(I) \le \epsilon\,\boldsymbol{a}(u_h;e_\kappa,e_\kappa) + \frac{1}{4\epsilon}\boldsymbol{a}(u_h;w,w),$$

and using the definition (2.2) of $\boldsymbol{a}(u_h;\cdot,\cdot)$, we get

$$\boldsymbol{a}(u_h;w,w) = \int_\Omega |\nabla w|^2 Q_h - \frac{1}{Q_h}|\nabla w\cdot\nabla u_h|^2\,dx \le \int_\Omega |\nabla w|^2 Q_h\,dx \le \|\nabla w\|_\infty^2 A_h(t).$$

Therefore,

$$(I) \le \epsilon\,\boldsymbol{a}(u_h;e_\kappa,e_\kappa) + \frac{1}{4\epsilon}\|\nabla w\|_\infty^2 A_h(t).$$

We now turn to estimate (II). Using the equivalent form (2.7) for $\boldsymbol{a}$, we have

$$(II) = \int_\Omega \nabla\kappa^T \left((Q-Q_h)I - \big(\frac{\nabla u\otimes\nabla u}{Q} - \frac{\nabla u_h\otimes\nabla u_h}{Q_h}\big)\right)\nabla w\,dx$$

By (4.1) and (4.2), the integrand in (II) is bounded by $4\,Q\,Q_h\,|\nabla\kappa|\,|\nabla w|\,|\nu-\nu_h|$, which by Cauchy-Schwarz inequality gives

$$\begin{aligned}(II) &\le 4\int_\Omega Q^2|\nabla\kappa|^2|\nabla w|^2 Q_h\,dx + \int_\Omega |\nu-\nu_h|^2 Q_h\,dx\\ &\le 4\|Q\|_\infty^2\|\nabla\kappa\|_\infty^2\|\nabla w\|_\infty^2 A_h(t) + N_h(t).\end{aligned}$$

Since $A_h(t) \le C$ from (3.6), the bounds for (I) and (II) yield the assertion. □

LEMMA 4.4 (Consistency estimate for $\tilde{\boldsymbol{a}}$). *For every $\epsilon > 0$ we have*

$$|\tilde{\boldsymbol{a}}(u;u,w) - \tilde{\boldsymbol{a}}(u_h;u_h,w)| \le \epsilon\tilde{\boldsymbol{a}}(u_h;w,w) + \frac{1}{4\epsilon}N_h(t), \qquad \forall w\in\mathcal{X}.$$

Proof. Using the definition (2.3) of $\tilde{\boldsymbol{a}}$ and Cauchy-Schwarz inequality, we obtain

$$\begin{aligned}|\tilde{\boldsymbol{a}}(u;u,w) - \tilde{\boldsymbol{a}}(u_h;u_h,w)| &\le \int_\Omega \Big|\frac{\nabla u}{Q} - \frac{\nabla u_h}{Q_h}\Big|\,|\nabla w|\,dx \le \int_\Omega |\nu-\nu_h|\,|\nabla w|\,dx\\ &\le \epsilon\int_\Omega \frac{|\nabla w|^2}{Q_h}\,dx + \frac{1}{4\epsilon}N_h(t) = \epsilon\,\tilde{\boldsymbol{a}}(u_h;w,w) + \frac{1}{4\epsilon}N_h(t),\end{aligned}$$

which is the desired estimate. □

The following lemma establishes another consistency estimate for $\boldsymbol{a}$, this time provided solely the *nonlinear* part of $\boldsymbol{a}$ changes.

LEMMA 4.5. *There exists a constant $C = C(\|Q\|_\infty) > 0$ such that for every $\epsilon > 0$*

$$|\boldsymbol{a}(u; v, w) - \boldsymbol{a}(u_h; v, w)| \leq \epsilon\, \boldsymbol{a}(u_h; w, w) + \frac{C}{\epsilon}\|\nabla v\|_\infty^2 N_h(t), \quad \forall v, w \in \mathcal{X}.$$

Proof. With $R := \|Q\|_\infty$, we consider the following disjoint splitting of Ω: $\Omega = \Omega^+ \cup \Omega^-$ with $\Omega^+ := \{x \in \Omega \,|\, Q_h(x) > 2R\}$ and $\Omega^- := \{x \in \Omega \,|\, Q_h(x) \leq 2R\}$.

We first estimate the integrand of $\boldsymbol{a}(u; \cdot, \cdot) - \boldsymbol{a}(u_h; \cdot, \cdot)$ in case $x \in \Omega^-$. According to (2.7), we consider this integrand written in the form

$$\nabla v^T \Big((Q - Q_h) I - \big(\frac{\nabla u \otimes \nabla u}{Q} - \frac{\nabla u_h \otimes \nabla u_h}{Q_h} \big) \Big) \nabla w =: (I).$$

Since $Q_h(x) \leq 2R$ for $x \in \Omega^-$, in view of (4.1) and (4.2) we have

$$\begin{aligned}(I) &\leq 4|\nabla v|\,|\nabla w|\,Q\,Q_h|\nu - \nu_h| \leq 8R^2|\nabla v|\frac{|\nabla w|}{\sqrt{Q_h}}|\nu - \nu_h|\sqrt{Q_h} \\ &\leq \epsilon\frac{|\nabla w|^2}{Q_h} + 16\frac{R^4}{\epsilon}\|\nabla v\|_\infty^2|\nu - \nu_h|^2 Q_h.\end{aligned}$$

To analyze the case $x \in \Omega^+$, we choose ζ, ζ_h, χ_i, $\chi_{h,i}$ as in Remark 2.4. Since $Q(x) \leq R$ and $Q_h(x) > 2R$ we have

$$|\nu - \nu_h| \geq \frac{1}{Q} - \frac{1}{Q_h} \geq \frac{1}{2R} \qquad \text{and} \qquad |\zeta - \zeta_h|\,,\, |\chi_i - \chi_{h,i}| \leq 2 \leq 4R|\nu - \nu_h|. \quad (4.4)$$

Consider the integrand in the form (2.6)

$$\underbrace{\big(\frac{\nabla v\cdot\zeta\,\nabla w\cdot\zeta}{Q} - \frac{\nabla v\cdot\zeta_h\,\nabla w\cdot\zeta_h}{Q_h}\big)}_{(II)} + \sum_{i=1}^{d-1} \underbrace{\nabla w^T\big(\chi_i \otimes \chi_i\, Q - \chi_{h,i} \otimes \chi_{h,i}\, Q_h\big)\nabla v}_{(III)_i}.$$

Since $R \geq 1$, we have for (II)

$$\begin{aligned}(II) &= \nabla v^T\big(\frac{\zeta\otimes\zeta}{Q} - \frac{\zeta_h\otimes\zeta_h}{Q_h}\big)\nabla w \\ &= \nabla v^T\left[(\zeta - \zeta_h)\otimes\zeta\frac{1}{Q} + \zeta_h\otimes\zeta\big(\frac{1}{Q} - \frac{1}{Q_h}\big) + \zeta_h\otimes(\zeta - \zeta_h)\frac{1}{Q_h}\right]\nabla w \\ &\leq C\,R\,|\nabla v|\,|\nabla w|\,|\nu - \nu_h| \leq \frac{C^2\,R^2}{4\epsilon}\|\nabla v\|_\infty^2|\nu - \nu_h|^2 Q_h + \epsilon\frac{|\nabla w|^2}{Q_h}.\end{aligned}$$

For $(III)_i$, instead, we proceed as follows with the aid of (4.1):

$$\begin{aligned}(III)_i &= \nabla w^T\Big((\chi_i - \chi_{h,i})\otimes\chi_i\,Q + \chi_{h,i}\otimes\chi_i\,(Q - Q_h) + \chi_{h,i}\otimes(\chi_i - \chi_{h,i})Q_h\Big)\nabla v \\ &\leq 4\,R^2\,|\nu - \nu_h|\,|\nabla v|\,|\nabla w| + 5R\,|\nu - \nu_h|Q_h|\chi_{h,i}\cdot\nabla w|\,|\nabla v| \\ &\leq \epsilon\frac{|\nabla w|^2}{Q_h} + \epsilon|\nabla w\cdot\chi_{h,i}|^2 Q_h + \frac{CR^4}{\epsilon}\|\nabla v\|_\infty^2|\nu - \nu_h|^2 Q_h.\end{aligned}$$

Collecting the estimates for both cases $x \in \Omega^-$ and $x \in \Omega^+$, integrating over Ω and recalling (2.6), we obtain the assertion after relabeling ϵ. ☐

Using Lemma 4.5 we obtain a coercivity estimate for $\boldsymbol{a}$.

COROLLARY 4.6 (Coercivity of $\boldsymbol{a}$). *There exists $C = C(\|Q\|_\infty) > 0$ such that*

$$\boldsymbol{a}(u;\kappa,e_\kappa) - \boldsymbol{a}(u_h;\kappa_h,e_\kappa) \geq \frac{1}{2}\boldsymbol{a}(u_h;e_\kappa,e_\kappa) - C\|\nabla\kappa\|_\infty^2 N_h(t).$$

Proof. Adding and subtracting $\boldsymbol{a}(u_h;\kappa,e_\kappa)$, and using Lemma 4.5 with $\epsilon = 1/2$, we readily obtain the desired estimate. ☐

LEMMA 4.7 (Coercivity of $N_h(t)$). *There exists $C = C(\|Q\|_\infty)$ such that*

$$\boldsymbol{a}(u_h;e_u,e_u) \leq C N_h(t).$$

Proof. In light of Remark 2.4, we can write

$$\boldsymbol{a}(u_h;e_u,e_u) = \int_\Omega \underbrace{\frac{|\nabla e_u\cdot\zeta_h|^2}{Q_h}}_{(I)}\,dx + \sum_{i=1}^{d-1}\int_\Omega \underbrace{|\nabla e_u\cdot\chi_{h,i}|^2\,Q_h}_{(II)_i}\,dx.$$

By virtue of (4.1), (I) satisfies

$$\begin{aligned}(I) &\leq \frac{|\nabla e_u|^2}{Q_h} = \frac{|\nabla u - \nabla u_h|^2}{Q_h} \leq \frac{|\nu Q - \nu_h Q_h|^2}{Q_h}\\ &\leq \frac{|\nu(Q-Q_h) + (\nu-\nu_h)Q_h|^2}{Q_h} \leq 4\|Q\|_\infty^2\,Q_h|\nu-\nu_h|^2.\end{aligned} \tag{4.5}$$

To treat the integrand $(II)_i$ we again split Ω into Ω^- and Ω^+, as in Lemma 4.5. Consider first $x \in \Omega^-$, namely $Q_h(x) \leq 2R$ with $R := \|Q(t)\|_\infty$. As in (4.5), we get

$$|\nabla e_u\cdot\chi_{h,i}|^2 Q_h \leq 4R^2\frac{|\nabla e_u|^2}{Q_h} \leq 16\|Q\|_\infty^4 Q_h|\nu-\nu_h|^2.$$

Now we consider $Q_h(x) > 2R$. Since $\nabla u_h\cdot\chi_{h,i} = 0$, it follows from (4.4) that

$$\nabla e_u\cdot\chi_{h,i} = \nabla(u-u_h)\cdot\chi_{h,i} = \nabla u\cdot\chi_{h,i} \leq |\nabla u| \leq 2\,R\,\|\nabla u\|_\infty\,|\nu-\nu_h|,$$

whence

$$|\nabla e_u\cdot\chi_{h,i}|^2 Q_h \leq 4\|Q\|_\infty^4|\nu-\nu_h|^2 Q_h.$$

The desired estimate then follows by integration over Ω. ☐

5. A Priori Error Analysis. In this section we prove the main theoretical result of this article, which can be stated as follows:

THEOREM 5.1. *Let (u_h,κ_h) be the semidiscrete solution of Definition 3.1, and let $e_u := u - u_h$, $e_\kappa := \kappa - \kappa_h$. There exists a constant C depending on $\|\nabla f\|_\infty$, $\|\partial_t u\|_{L^2(H^{k+1}(\Omega))}$, $\|\partial_t\nabla u\|_\infty$, $\|\kappa\|_{L^2(H^{k+1}(\Omega))}$, $\|\partial_t\kappa\|_{L^2(H^k(\Omega))}$, and $\|\nabla\kappa\|_\infty$, such that*

$$\sup_{s\in[0,T]}\left(\|e_u(s)\|_2^2 + \int_{\Gamma_h(s)}|\nabla_S e_u(s)|^2\right) + \int_0^T\left(\|e_\kappa(s)\|_2^2 + \int_{\Gamma_h(s)}|\nabla_S e_\kappa(s)|^2\right)ds \leq C\,h^{2k}.$$

The proof of Theorem 5.1 is a consequence of two estimates, the strong and the weak estimates, derived from the error equations (5.1) and (5.2) below by choosing appropriate test functions.

5.1. Proof of Theorem 5.1. Subtracting (3.2) and (3.3) from (2.4) and (2.5), respectively, we get the following error equations:

$$\langle \partial_t e_u, \psi_h\rangle - \big(\boldsymbol{a}(u;\kappa,\psi_h) - \boldsymbol{a}(u_h;\kappa_h,\psi_h)\big) = \boldsymbol{a}(u;f,\psi_h) - \boldsymbol{a}(u_h;f,\psi_h) \tag{5.1}$$

$$\langle e_\kappa, \varphi_h\rangle + \big(\tilde{\boldsymbol{a}}(u;u,\varphi_h) - \tilde{\boldsymbol{a}}(u_h;u_h,\varphi_h)\big) = 0, \tag{5.2}$$

for all $\psi_h, \varphi_h \in \mathcal{X}_h$. The strong and weak estimates below are formulated in terms of the following interpolation errors, which can be bounded via (3.1):

$$\rho_u := u - I_h u, \qquad \rho_\kappa := \kappa - I_h \kappa_h. \tag{5.3}$$

The strong estimate of §5.2 reads as follows: *For all $\epsilon > 0$ there exists a constant C_0 depending only on $\|\nabla f\|_\infty, \|\nabla\kappa\|_\infty, \|\partial_t \nabla u\|_\infty$, and ϵ, such that for $t \in [0,T]$*

$$\begin{aligned} N_h(t) + \int_0^t \boldsymbol{a}(u_h; e_\kappa, e_\kappa)\, ds \le N_h(0) &+ C_0 \int_0^t \Big(N_h(s) + \|e_u(s)\|_2^2\Big)\, ds \\ &+ 2\epsilon\Big(\|e_u(t)\|_2^2 + \int_0^t \|e_\kappa(s)\|_2^2\, ds\Big) \\ &+ \frac{1}{2\epsilon}\|\rho_\kappa(t)\|_2^2 + \|e_u(0)\|_2^2 + \|\rho_\kappa(0)\|_2^2 \\ &+ C_0 \int_0^t \Big(\|\nabla\rho_\kappa\|_\infty^2 + \|\partial_t\nabla\rho_u\|_2^2 + \|\partial_t\rho_u\|_2^2 + \|\partial_t\rho_\kappa\|_2^2\Big)\, ds. \end{aligned} \tag{5.4}$$

It is clear that to close the argument we need separate control on the term multiplied by ϵ of the right-hand side of (5.4). This is provided by the weak estimate of §5.3, which reads: *There exist constants C_1, C_2 depending on $\|\nabla f\|_\infty$ and $\|Q\|_\infty$ such that for $t \in [0,T]$ we have*

$$\begin{aligned} \frac{1}{2}\|e_u(t)\|_2^2 + \int_0^t \|e_\kappa(s)\|_2^2\, ds \le \frac{1}{2}\|e_u(0)\|_2^2 &+ \int_0^t \|e_u(s)\|_2^2\, ds \\ &+ C_1 \int_0^t N_h(s)\, ds + \frac{1}{2}\int_0^t \boldsymbol{a}(u_h; e_\kappa, e_\kappa)\, ds \\ &+ \int_0^t \Big(\|\nabla\rho_\kappa(s)\|_2^2 + \|\rho_\kappa(s)\|_2^2 + \|\partial_t\rho_u(s)\|_2^2\Big)\, ds \\ &+ 2\|\rho_u(t)\|_2^2 + C_2 \int_0^t \|\nabla\rho_u(s)\|_\infty^2\, ds. \end{aligned} \tag{5.5}$$

To prove Theorem 5.1 we add (5.4) and (5.5), and then choose $\epsilon = 1/8$ to eliminate $\|e_u(t)\|_2^2 + \int_0^t \|e_\kappa(s)\|_2^2\, ds$ from the right-hand side. Employing a Gronwall argument, we can also remove $\int_0^t \big(N_h(s) + \|e_u(s)\|_2^2\big)\, ds$ from the right-hand side at the expense of an exponential depending on C_0, C_1 and T. Finally, Lemma 4.7, in conjunction with $\boldsymbol{a}(u_h; v, v) = \int_{\Gamma_h} \nabla_S v \cdot \nabla_S v$, yields the left-hand side of the asserted estimate. Its right-hand side, and underlying a priori regularity, result from applying (3.1) to the terms involving ρ_κ, ρ_u defined in (3.1).

5.2. Strong Estimate (5.4)**.** To prove (5.4), we choose the discrete functions

$$\begin{aligned} -\psi_h &:= I_h\kappa - \kappa_h = (\kappa - \kappa_h) + (I_h\kappa - \kappa) = e_\kappa - \rho_\kappa \in \mathcal{X}_h \\ \varphi_h &:= \partial_t(I_h u - u_h) = \partial_t e_u - \partial_t \rho_u \in \mathcal{X}_h. \end{aligned}$$

Adding (5.1) and (5.2), and invoking Lemma 4.2 and Corollary 4.6, we get

$$\begin{aligned}
&\frac{1}{2}\partial_t N_h(t)+\frac{1}{2}\boldsymbol{a}(u_h;e_\kappa,e_\kappa) - C\,N_h(t)\\
&\qquad\le \boldsymbol{a}(u;\kappa,e_\kappa) - \boldsymbol{a}(u_h;\kappa_h,e_\kappa) + \tilde{\boldsymbol{a}}(u;u,\partial_t e_u) - \tilde{\boldsymbol{a}}(u_h;u_h,\partial_t e_u)\\
&\qquad= \big(\boldsymbol{a}(u;\kappa,\rho_\kappa) - \boldsymbol{a}(u_h;\kappa_h,\rho_\kappa)\big) - \big(\boldsymbol{a}(u;f,e_\kappa-\rho_\kappa) - \boldsymbol{a}(u_h;f,e_\kappa-\rho_\kappa)\big)\\
&\qquad\quad + \big(\tilde{\boldsymbol{a}}(u;u,\partial_t\rho_u) - \tilde{\boldsymbol{a}}(u_h;u_h,\partial_t\rho_u)\big) - \langle\partial_t e_u,\rho_\kappa\rangle + \langle e_\kappa,\partial_t\rho_u\rangle\\
&\qquad=: (I)+(II)+(III)+(IV)+(V),
\end{aligned}$$

with C depending only on $\|\partial_t\nabla u\|_\infty$, $\|\nabla\kappa\|_\infty$, and $\|Q\|_\infty$, and $\|Q\|_\infty$. We now proceed to estimate each term on the right-hand side separately.

By Lemma 4.3, there is a constant $C = C(\epsilon,\|\nabla\kappa\|_\infty,\|Q\|_\infty,\|\nabla f\|_\infty)$, such that

$$\big|(I)\big| \le \epsilon\,\boldsymbol{a}(u_h;e_\kappa,e_\kappa) + C\|\nabla\rho_\kappa\|_\infty^2 + N_h(t).$$

Using Lemma 4.4 with $\epsilon = 1$, we obtain

$$\big|(III)\big| \le \tilde{\boldsymbol{a}}(u_h;\partial_t\rho_u,\partial_t\rho_u) + N_h(t) \le \|\nabla\partial_t\rho_u\|_2^2 + N_h(t).$$

For any $t\in[0,T]$ we integrate (IV) by parts on $[0,t]$, thereby obtaining

$$\begin{aligned}
\int_0^t (IV)(s)\,ds &= \langle e_u(0),\rho_\kappa(0)\rangle - \langle e_u(t),\rho_\kappa(t)\rangle + \int_0^t \langle e_u(s),\partial_t\rho_\kappa(s)\rangle\,ds\\
&\le \frac{1}{2}\|e_u(0)\|_2^2 + \frac{1}{2}\|\rho_\kappa(0)\|_2^2 + \frac{\epsilon}{2}\|e_u(t)\|_2^2 + \frac{1}{2\epsilon}\|\rho_\kappa(t)\|_2^2\\
&\quad + \frac{1}{2}\int_0^t \Big(\|e_u(s)\|_2^2 + \|\partial_t\rho_\kappa(s)\|_2^2\Big)\,ds.
\end{aligned}$$

For (V) we readily have

$$\big|(V)\big| \le \frac{\epsilon}{2}\|e_\kappa\|_2^2 + \frac{1}{2\epsilon}\|\partial_t\rho_u\|_2^2.$$

We decompose (II) into discretization and interpolation errors as follows:

$$-(II) = \underbrace{\big(\boldsymbol{a}(u;f,e_\kappa) - \boldsymbol{a}(u_h;f,e_\kappa)\big)}_{(II)_e} - \underbrace{\big(\boldsymbol{a}(u;f,\rho_\kappa) - \boldsymbol{a}(u_h;f,\rho_\kappa)\big)}_{(II)_\rho}. \tag{5.6}$$

In light of Lemma 4.5, there is a constant $C = C(\|Q\|_\infty)$ such that

$$\big|(II)_e\big| \le \frac{1}{4}\,\boldsymbol{a}(u_h;e_\kappa,e_\kappa) + C\|\nabla f\|_\infty^2 N_h(t).$$

Using Lemma 4.1 and (3.6), we find a constant $C = C(\|\nabla f\|_\infty,\|Q\|_\infty,A_h(0))$ such that

$$\begin{aligned}
\big|(II)_\rho\big| &= \Big|\int_\Omega \nabla f^T\Big((Q-Q_h)I - \big(\frac{\nabla u\otimes\nabla u}{Q} - \frac{\nabla u_h\otimes\nabla u_h}{Q_h}\big)\Big)\nabla\rho_\kappa\,dx\Big|\\
&\le 4\int_\Omega |\nabla f|\,|\nabla\rho_\kappa|\,Q\,Q_h\,|\nu-\nu_h|\,dx\\
&\le 4\|\nabla f\|_\infty^2\|\nabla\rho_\kappa\|_\infty^2\|Q\|_\infty^2\int_\Omega Q_h\,dx + \int_\Omega |\nu-\nu_h|^2 Q_h\,dx\\
&\le C\|\nabla\rho_\kappa\|_\infty^2 A_h(t) + N_h(t) \le C\|\nabla\rho_\kappa\|_\infty^2 + N_h(t).
\end{aligned}$$

Finally, collecting the above estimates for (I) to (V), subtracting $\frac{1}{4}\,\boldsymbol{a}(u_h;e_\kappa,e_\kappa)$ and integrating in time from 0 to $t\in[0,T]$, we arrive at (5.4).

5.3. Weak Estimate (5.5)**.** To prove (5.5), we choose the discrete functions

$$\begin{aligned}\psi_h &:= I_h u - u_h = e_u - \rho_u \in \mathcal{X}_h,\\ \varphi_h &:= I_h \kappa - \kappa_h = e_\kappa - \rho_\kappa \in \mathcal{X}_h.\end{aligned}$$

Adding the error equations (5.1) and (5.2), we obtain

$$\begin{aligned}\langle \partial_t e_u, e_u\rangle + \langle e_\kappa, e_\kappa\rangle &= \big(\boldsymbol{a}(u;\kappa,e_u) - \boldsymbol{a}(u_h;\kappa_h,e_u)\big) - \big(\tilde{\boldsymbol{a}}(u;u,e_\kappa) - \tilde{\boldsymbol{a}}(u_h;u_h,e_\kappa)\big)\\ &\quad + \langle \partial_t e_u, \rho_u\rangle - \big(\boldsymbol{a}(u;\kappa,\rho_u) - \boldsymbol{a}(u_h;\kappa_h,\rho_u)\big)\\ &\quad + \big(\boldsymbol{a}(u;f,e_u-\rho_u) - \boldsymbol{a}(u_h;f,e_u-\rho_u)\big) + \langle e_\kappa,\rho_\kappa\rangle\\ &\quad + \big(\tilde{\boldsymbol{a}}(u;u,\rho_\kappa) - \tilde{\boldsymbol{a}}(u_h;u_h,\rho_\kappa)\big)\\ &=: (I)+\cdots+(VII).\end{aligned} \tag{5.7}$$

We proceed now to bound each term from (I) to (VII) separately.

Adding and subtracting $\boldsymbol{a}(u_h;\kappa,e_u)$ to (I), and employing Lemma 4.5 with $\epsilon = \frac{1}{6}$, we readily have

$$\begin{aligned}\big|(I)\big| &\le \big|\boldsymbol{a}(u;\kappa,e_u) - \boldsymbol{a}(u_h;\kappa,e_u)\big| + \big|\boldsymbol{a}(u_h;e_\kappa,e_u)\big|\\ &\le C\|\nabla\kappa\|_\infty^2 N_h(t) + \frac{5}{2}\,\boldsymbol{a}(u_h;e_u,e_u) + \frac{1}{6}\,\boldsymbol{a}(u_h;e_\kappa,e_\kappa).\end{aligned}$$

Consequently, Lemma 4.7 yields the following bound with $C = C(\|\nabla\kappa\|_\infty, \|Q\|_\infty)$

$$\big|(I)\big| \le C N_h(t) + \frac{1}{6}\,\boldsymbol{a}(u_h;e_\kappa,e_\kappa).$$

Making use of Lemma 4.4 and Remark 2.3, we readily deduce (using $\epsilon = \frac{1}{6}$)

$$\big|(II)\big| \le \frac{1}{6}\,\tilde{\boldsymbol{a}}(u_h;e_\kappa,e_\kappa) + \frac{3}{2}N_h(t) \le \frac{1}{6}\,\boldsymbol{a}(u_h;e_\kappa,e_\kappa) + \frac{3}{2}N_h(t),$$

as well as (using $\epsilon = \frac{1}{2}$)

$$\big|(VII)\big| \le \frac{1}{2}\tilde{\boldsymbol{a}}(u_h;\rho_\kappa,\rho_\kappa) + \frac{1}{2}N_h(t) \le \frac{1}{2}\|\nabla\rho_\kappa\|_2^2 + \frac{1}{2}N_h(t).$$

Using Lemma 4.3 with $\epsilon = \frac{1}{6}$ we find a constant $C = C(\|\nabla\kappa\|_\infty, \|Q\|_\infty, \|\nabla f\|_\infty)$ such that

$$\big|(IV)\big| \le \frac{1}{6}\,\boldsymbol{a}(u_h;e_\kappa,e_\kappa) + N_h(t) + C\|\nabla\rho_u\|_\infty^2.$$

For (VI), we obviously have $\big|(VI)\big| \le \frac{1}{2}\,\|e_\kappa\|_2^2 + \frac{1}{2}\|\rho_\kappa\|_2^2$. For (III), instead, we integrate by parts on $[0,t]$ for any $t \in [0,T]$, to obtain

$$\begin{aligned}\int_0^t (III)\,ds &= \langle e_u(t),\rho_u(t)\rangle - \langle e_u(0),\rho_u(0)\rangle - \int_0^t \langle e_u(s),\partial_t\rho_u(s)\rangle\,ds\\ &\le \frac{1}{4}\,\|e_u(t)\|_2^2 + \|\rho_u(t)\|_2^2 + \frac{1}{2}\int_0^t \|e_u(s)\|_2^2 + \|\partial_t\rho_u(s)\|_2^2\,ds.\end{aligned}$$

It remains to bound (V), which involves the right-hand side f. Applying Lemma 4.5 (with $\epsilon = 1$) and Lemma 4.7, we obtain

$$\big|\boldsymbol{a}(u;f,e_u) - \boldsymbol{a}(u_h;f,e_u)\big| \le C\|\nabla f\|_\infty^2 N_h(t) + \boldsymbol{a}(u_h;e_u,e_u) \le C N_h(t),$$

with $C = C(\|\nabla f\|_\infty, \|Q\|_\infty)$. Since $\boldsymbol{a}(u; f, \rho_u) - \boldsymbol{a}(u_h; f, \rho_u)$ is similar to $(II)_\rho$ in (5.6), we likewise deduce

$$\big|\boldsymbol{a}(u; f, \rho_u) - \boldsymbol{a}(u_h; f, \rho_u)\big| \le C\|\nabla\rho_u\|_\infty^2 A_h(t) + N_h(t) \le C\|\nabla\rho_u\|_\infty^2 + N_h(t),$$

whence, for C depending on $\|\nabla f\|_\infty$ and $\|Q\|_\infty$, we end up with

$$\big|(V)\big| \le C\|\nabla\rho_u\|_\infty^2 + CN_h(t).$$

Inserting the above bounds for (I) to (VII) back into (5.7), and integrating from 0 to t, we finally obtain the desired estimate (5.5).

6. Full Discretization. In this section we introduce the fully discrete scheme actually used in simulations, along with the linear algebra approach to its solution.

6.1. Definition and Properties. To discretize in time we subdivide the time interval into $t_0 = 0 < t_1 \cdots < t_N = T$ and set $\tau_n := t_{n+1} - t_n$. We define the notion of *semi-implicit* fully discrete problem as follows: Set $u_h^0 = u_h(0)$ and for $n = 0, 1, \ldots, N-1$ determine u_h^{n+1}, $\kappa_h^{n+1} \in \mathcal{X}_h$ by

$$\langle u_h^{n+1}, \psi_h\rangle - \tau_n \boldsymbol{a}(u_h^n; \kappa_h^{n+1}, \psi_h) = \tau_n \boldsymbol{a}(u_h^n; f^n, \psi_h) + \langle u_h^n, \psi\rangle \qquad \forall\ \psi_h \in \mathcal{X}_h, \tag{6.1}$$

$$\langle \kappa_h^{n+1}, \varphi_h\rangle + \tilde{\boldsymbol{a}}(u_h^n; u_h^{n+1}, \varphi_h) = 0 \qquad \forall\ \varphi_h \in \mathcal{X}_h, \tag{6.2}$$

with $f^n := f(t_n)$. Existence and uniqueness of solutions u_h^n, κ_h^n follows from the considerations in Section 6.2.

We now establish a stability estimate analogous to (3.6) in Lemma 2.6.

THEOREM 6.1 (Fully Discrete Stability). *Let $(u_h^n, \kappa_h^n)_{n=0}^N$ be a solution of the fully discrete equations (6.1) and (6.2), and let $A_h^n := \int_\Omega Q(u_h^n)dx$ denote the area of the surface $\Gamma_h^n := \{(x, u_h^n(x) \mid x \in \Omega\}$. There exists $C = C(\|\nabla f\|_\infty, A_h^0)$, such that*

$$\sup_{1\le n\le N} A_h^n + \sum_{n=1}^N \tau_n \int_{\Gamma_h^{n-1}} |\nabla_S \kappa_h^n|^2 \le C. \tag{6.3}$$

Moreover, if $f \equiv 0$, A_h^n is a decreasing sequence (strictly if $\boldsymbol{a}(u_h^{n-1}; \kappa_h^n, \kappa_h^n) > 0$).

Proof. Choose as test functions $-\kappa_h^{n+1}$ and $(u_h^{n+1} - u_h^n)$ in (6.1) and (6.2), respectively, and add both equations. One readily gets

$$\tau_n \boldsymbol{a}(u_h^n; \kappa_h^{n+1}, \kappa_h^{n+1}) + \int_\Omega \frac{\nabla u_h^{n+1} \cdot \nabla(u_h^{n+1} - u_h^n)}{Q(u_h^n)} = -\tau_n \boldsymbol{a}(u_h^n; f^n, \kappa_h^{n+1}). \tag{6.4}$$

The next step consists of finding a discrete counterpart of (3.7). Observing that

$$|a| - |b| \le \frac{a \cdot (a-b)}{|b|}, \qquad \forall a, b \in \mathbb{R}^{d+1},$$

and setting $a := (\nabla u_h^{n+1}, 1)^T$, $b := (\nabla u_h^n, 1)^T$, we obtain

$$Q(u_h^{n+1}) - Q(u_h^n) \le \frac{\nabla u_h^{n+1} \cdot \nabla(u_h^{n+1} - u_h^n)}{Q(u_h^n)}.$$

Inserting this into (6.4) gives $A_h^{n+1} \le A_h^n$, if $f \equiv 0$. To prove (6.3) for $f \not\equiv 0$, we have to bound the right-hand side in (6.4). This can be done similarly to (3.5), obtaining

$$|\boldsymbol{a}(u_h^n; f^n, \kappa_h^{n+1})| \le C(1 + A_h^n) \ + \ \epsilon\, \boldsymbol{a}(u_h^n; \kappa_h^{n+1}, \kappa_h^{n+1})$$

with $C = C(\epsilon, \|\nabla f\|_\infty)$. Multiplying by τ_n, choosing ϵ sufficiently small, summing up over all n, and using a discrete Gronwall argument, the result follows. ∎

6.2. Schur Complement Strategy. Let $\mathcal{X}_h = \operatorname{span}\{\varphi_j\} \subseteq \mathcal{X}$ with the usual nodal basis functions φ_j and the corresponding nodal space $\underline{\mathbf{X}}$. Then, for the time instant t_{n+1} the fully discrete system of equations can be rewritten as

$$\begin{bmatrix} \tilde{A} & M \\ M^T & -\tau A \end{bmatrix} \begin{bmatrix} \underline{U}^{n+1} \\ \underline{K}^{n+1} \end{bmatrix} = \begin{bmatrix} 0 \\ M^T \underline{U}^n + \tau \underline{F}^n \end{bmatrix}, \tag{6.5}$$

where $\underline{U}^n$, $\underline{K}^n$ denote the vector of nodal values for u_h^n, κ_h^n respectively,

$$u_h^n = \sum_j \underline{U}_j^n \, \varphi_j, \qquad \kappa_h^n = \sum_j \underline{K}_j^n \, \varphi_j,$$

the vector $\underline{F}^n$ is given by $\underline{F}_j^n = \boldsymbol{a}(u_h^n; f^n, \varphi_j)$, and the matrices M, A, $\tilde{A}$ are given by

$$M_{i,j} = \langle \psi_j, \varphi_i \rangle, \qquad A_{i,j} = \boldsymbol{a}(u_h^n; \psi_j, \psi_i), \qquad \tilde{A}_{i,j} = \tilde{\boldsymbol{a}}(u_h^n; \varphi_j, \varphi_i).$$

Notice that the matrices A and $\tilde{A}$ depend on u_h^n and thus have to be reassembled in every timestep.

To derive a Schur complement formulation, we have to distinguish between the various boundary conditions (see §2.2).

Dirichlet boundary conditions. In this case, since $\mathcal{X} := \mathring{H}^1(\Omega)$, the matrix $\tilde{A}$ is invertible, and a Schur complement for $\underline{K}^{n+1}$ is thus given by

$$\begin{aligned} \left(M^T \tilde{A}^{-1} M \; + \; \tau A \right) \underline{K}^{n+1} &= -M^T \underline{U}^n - \tau \underline{F}^n, \\ \tilde{A} \, \underline{U}^{n+1} &= -M \, \underline{K}^{n+1}. \end{aligned}$$

This system is decoupled and uniquely solvable for both $\underline{K}^{n+1}$ and $\underline{U}^{n+1}$.

Periodic and Neumann Boundary Conditions. This case is a bit more involved because constant functions are in $\mathcal{X}_h$, whence $\tilde{A}$ has a kernel $\ker(\tilde{A}) = \operatorname{span}\{\underline{1}\}$.

Let $\underline{\mathbf{V}}, \underline{\mathbf{W}} \subseteq \underline{\mathbf{X}}$ be the spaces of nodal values for $\underline{U}^{n+1}$ defined by

$$\underline{\mathbf{V}} := \{\underline{V} \mid \underline{1} \cdot MV = 0\}, \qquad \underline{\mathbf{W}} := \{\underline{V} \mid \underline{1} \cdot \underline{V} = 0\} = \operatorname{span}\{\underline{1}\}^{\perp}.$$

Multiplying the first equation in (6.5) by $\underline{1}$, we see that $\underline{1} \cdot M\underline{K}^{n+1} = 0$, which means that $\underline{K}^{n+1} \in \underline{\mathbf{V}}$. Let P be the orthogonal projection onto $\operatorname{span}\{\underline{1}\}$ with respect to the Euclidean inner product in $\mathbb{R}^I$. If $S := (\tilde{A}_{|\underline{\mathbf{W}}})^{-1}$, then

$$SM\underline{K}^{n+1} = -S\tilde{A}\underline{U}^{n+1} = -(I-P)\underline{U}^{n+1} = -\underline{U}^{n+1} + P\underline{U}^{n+1},$$

or $\underline{U}^{n+1} = -SM\underline{K}^{n+1} + P\underline{U}^{n+1}$. Consequently, using the second equation in (6.5)

$$(M^T SM + \tau A) \, \underline{K}^{n+1} - M^T P \, \underline{U}^{n+1} = -M^T \underline{U}^n - \tau \underline{F}^n. \tag{6.6}$$

Let now $\Pi := I - \dfrac{M^T\underline{1} \otimes M^T\underline{1}}{|M^T\underline{1}|^2}$ be the orthogonal projection onto $\underline{\mathbf{V}}$. Applying Π to both sides of (6.6) and using that $\Pi M P \underline{U}^{n+1} = 0$ and $\Pi \underline{K}^{n+1} = \underline{K}^{n+1}$, we arrive at

$$\Pi(M^T SM + \tau A)\Pi \, \underline{K}^{n+1} = -\Pi(M^T \underline{U}^n + \tau \underline{F}^n), \tag{6.7}$$

The matrix $\Pi(M^T SM + \tau A)\Pi$ is symmetric and positive definite in $\underline{\mathbf{V}}$ and thus (6.7) is uniquely solvable for $\underline{K}^{n+1}$ in $\underline{\mathbf{V}}$. Finally, $\underline{U}^{n+1}$ is uniquely determined by

$$\tilde{A} \, \underline{U}^{n+1} = -M \, \underline{K}^{n+1}, \qquad \underline{1} \cdot M^T \, \underline{U}^{n+1} = \underline{1} \cdot M^T \, \underline{U}^n. \tag{6.8}$$

Note that the last equation is the conservation of volume $\int_\Omega (U^{n+1} - U^n) = 0$ written in matrix-vector form; compare with Remark 2.5.

7. Numerical Experiments. The purpose of this section is to document via several experiments the performance of the discretization scheme proposed in this article. We open this section with some comments about the implementation of the algorithm within the flexible adaptive finite element toolbox ALBERT [15, 16]. We continue with a verification of the experimental orders of convergence (EOC) achieved by the method with different polynomial degrees and relations between timestep τ and meshsize h. We next illustrate the smoothing effect of surface diffusion (case $f = 0$), and we finally present simulations driven by a forcing term which exhibit singularity formation in finite time in both 1d and 2d (case $f \neq 0$).

7.1. Implementation. The matrices of Section 6 were assembled using the standard assembling tools of ALBERT, and the solution to the linear systems (6.7)–(6.8) were obtained by a conjugate gradient method.

For the assembling of the linear systems, quadrature rules exact for polynomials of degree $2k$ were used, where k is the degree of the finite element. For computing the errors versus the exact solution, quadratures of order $2k + 2$ were used.

For all the experiments presented in this article, domains with periodic boundary conditions were considered. Experiments with other boundary conditions were also carried out and will be shown elsewhere. The results were similar.

7.2. Experimental Orders of Convergence (EOC). To test the performance of the discretization scheme we consider the domain $\Omega = (-1, 1)\times(-1, 1) \subset \mathbb{R}^2$ with the exact solution

$$u(x, y, t) = 1 + 0.1 \sin(\pi x) \sin(2\pi y) \cos(\pi t), \qquad \forall\ t \in [0, 1].$$

The exact curvature $\kappa = \nabla\cdot\left(\frac{\nabla u}{Q}\right)$ and right hand side $F = \partial_t u - Q\Delta_S\kappa$ were obtained using the symbolic capabilities of Mathematica. The FEM of §6 is used to compute (u_h, κ_h) and compare them with (u, κ) in Tables 7.1–7.4. They display the errors

$$\mathrm{err}_\nu := \sup_{0\le t\le T}\left(\int_\Omega |\nu - \nu_h|^2 Q_h\right)^{1/2}, \qquad \mathrm{err}_u := \sup_{0\le t\le T} \boldsymbol{a}(u_h; e_u, e_u)^{1/2},$$

$$\mathrm{err}_\kappa := \left(\int_0^T \boldsymbol{a}(u_h; e_\kappa, e_\kappa)\right)^{1/2}, \quad \mathrm{err}_{u,2} := \sup_{0\le t\le T} \|e_u\|_2, \quad \mathrm{err}_{\kappa,2} := \left(\int_0^T \|e_\kappa\|^2\right)^{1/2},$$

for different values of h and τ along with the EOC's. Given two meshes with meshsizes H, h and errors err_H, err_h, respectively, the EOC is determined according to

$$\mathrm{EOC} = \frac{\log(\mathrm{err}_H/\mathrm{err}_h)}{\log(H/h)},$$

which gives the computational exponent k in the expression $\mathrm{err}_h \cong Ch^k$.

In Table 7.1 we show the results obtained using *linear* elements and a timestep $\tau = h$. Even though τ seems to be big as compared to h, the convergence rate is still linear and no instabilities arise. This is not so surprising if we recall that the fully discrete system is *unconditionally* stable (see Theorem 6.1). In order to verify the error analysis in §5 for the *semidiscretization in space*, we also compute the EOCs for smaller values of τ, namely $\tau = 0.1h$ and $\tau = h^2$; see Tables 7.2 and 7.3. Here again, we observe that the EOCs are at least 1. Moreover, as one would expect, the errors measured in $L^2(\Omega)$-norms are approximately of second order provided $\tau = h^2$;

h	err_ν	EOC	err_u	EOC	err_κ	EOC	$\mathrm{err}_{u,2}$	EOC	$\mathrm{err}_{\kappa,2}$	EOC
1/2	0.5601		0.6055		18.2		0.0836		2.1921	
1/4	0.2549	1.14	0.2884	1.07	7.70	1.24	0.0287	1.54	0.4366	2.33
1/8	0.1297	0.97	0.1448	0.99	4.66	0.73	0.0121	1.24	0.1773	1.30
1/16	0.0636	1.03	0.0708	1.03	2.41	0.95	0.0049	1.32	0.0630	1.49
1/32	0.0310	1.03	0.0344	1.04	1.21	0.99	0.0021	1.24	0.0262	1.26

TABLE 7.1
Linear elements, $\tau = h$

h	err_ν	EOC	err_u	EOC	err_κ	EOC	$\mathrm{err}_{u,2}$	EOC	$\mathrm{err}_{\kappa,2}$	EOC
1/2	0.5594		0.6048		18.4		0.0834		2.2249	
1/4	0.2463	1.18	0.2772	1.13	7.67	1.26	0.0251	1.73	0.4071	2.45
1/8	0.1240	0.99	0.1364	1.02	4.67	0.71	0.0081	1.62	0.1484	1.46
1/16	0.0611	1.02	0.0669	1.03	2.40	0.96	0.0022	1.87	0.0397	1.90
1/32	0.0304	1.01	0.0332	1.01	1.19	1.00	0.0006	1.85	0.0102	1.97

TABLE 7.2
Linear elements, $\tau = 0.1h$

this is not predicted by our theory though. For $\tau = h, 0.1h$ we do not recover second order errors because the time discretization error —expected to be of first order— dominates the space error in $L^2(\Omega)$-norms.

h	err_ν	EOC	err_u	EOC	err_κ	EOC	$\mathrm{err}_{u,2}$	EOC	$\mathrm{err}_{\kappa,2}$	EOC
1/2	0.5597		0.6051		18.4		0.0835		2.2214	
1/4	0.2470	1.18	0.2782	1.12	7.67	1.26	0.0254	1.71	0.4073	2.45
1/8	0.1240	0.99	0.1365	1.03	4.61	0.73	0.0082	1.63	0.1466	1.47
1/16	0.0611	1.02	0.0669	1.03	2.38	0.96	0.0022	1.93	0.0392	1.90
1/32	0.0304	1.01	0.0332	1.01	1.19	1.00	0.0005	1.98	0.0099	1.99

TABLE 7.3
Linear elements, $\tau = h^2$

To further verify experimentally the error estimates of §5, which are valid for any polynomial degree, we also compute the EOCs for *quadratic* elements. Table 7.4 displays the results obtained with quadratics and $\tau = h^2$. The EOCs are about 2 in all the error norms, as predicted by theory, including those in $L^2(\Omega)$. In fact, the latter cannot exhibit EOCs close to 3 due to the choice of the timestep $\tau = h^2$.

h	err_ν	EOC	err_u	EOC	err_κ	EOC	$\mathrm{err}_{u,2}$	EOC	$\mathrm{err}_{\kappa,2}$	EOC
1/2	0.1271		0.1376		7.38		0.0101		0.3277	
1/4	0.0419	1.60	0.0487	1.50	2.47	1.58	0.0040	1.35	0.0797	2.04
1/8	0.0102	2.03	0.0122	1.99	0.71	1.80	0.0009	2.19	0.0152	2.39
1/16	0.0025	2.01	0.0030	2.00	0.17	2.07	0.0002	2.11	0.0032	2.24

TABLE 7.4
Quadratic elements, $\tau = h^2$

7.3. Smoothing Effect in 1d: Case $f \equiv 0$. In this section we present experimental results in $\Omega = (-1, 1)$ concerning the behavior of the discrete solution when $f \equiv 0$ and $u_0(x) = 1 + \delta(x)$ is a perturbation of the stationary solution $u \equiv 1$.

Superposition of Sines. We consider the perturbation

$$\delta(x) = 0.1\,\sin(\pi x) + 0.3\,\sin(16\,\pi x), \tag{7.1}$$

which results from the superposition of two frequencies. We compute the approximate solution with linear elements and parameters $h = 1/128$, $\tau = 10^{-6}$. This choice of discretization parameters is necessary to reflect the intrinsic time scale for this example. Figure 7.1 depicts the solution for different time instants, and shows that

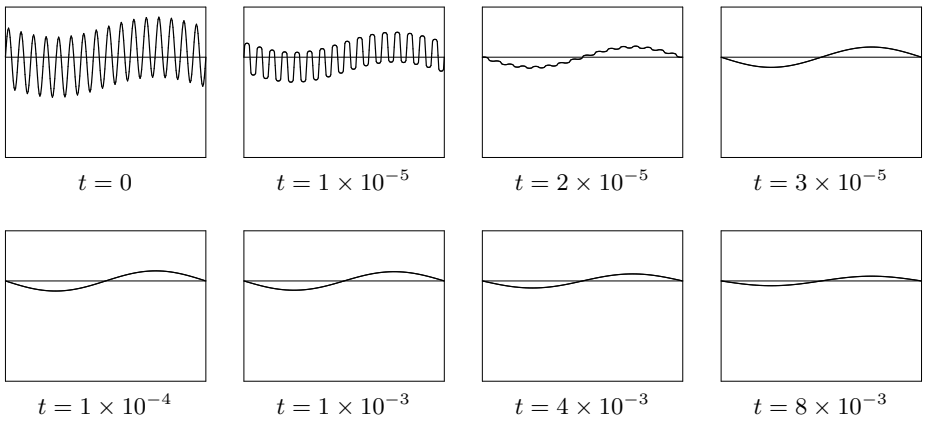

FIG. 7.1. *Solutions for $f \equiv 0$ and $u_0(x) = 1 + 0.1\sin(\pi x) + 0.3\sin(16\pi x)$ at various instants t. In all the plots, the x-axis ranges from -1 to 1, and the y-axis ranges from 0 to 1.5.*

high frequencies are rapidly damped, whereas the amplitude of low frequency waves decays *very* slowly. To quantify the difference in the timescales it is worth noting that the time elapsed between the first and the last plot of the first row of Figure 7.1 is 3×10^{-5} whereas that of the second row is almost 10^{-2}, a three orders of magnitude difference! This is related to the 4th order operator of surface diffusion.

Nonnegative Perturbation. Let the perturbation be $\delta(x) = 0.3\,\delta_0(0.15\,x)$ with

$$\delta_0(x) = \min(1, \max(0, 2 - |x|)), \tag{7.2}$$

which is nonnegative and rather singular for this 4th order flow because of its kinks (see Figure 7.2). We compute the approximate solution with linear elements, and parameters $h = 1/128$, $\tau = 10^{-6}$. Figure 7.2 displays the solution for different time instants and confirms the strong smoothing effect of surface diffusion alluded to before. Another important feature that can be visualized in Figure 7.2, is the lack of maximum principle for this equation: we start with a function $u_0 \geq 1$ and after the first time step, there are already points x with $u(x) < 1$. This is consistent with the 4th order structure of the operator. It is also worth observing that the spectrum of u_0 is rather full due to the kinks, and that high and low frequencies have drastically different decay rates.

Steep Perturbation. This example shows that global in time existence may not be expected for a classical solution of (1.1), thereby revealing some limitations of the graph formulation. For $K = 1 + \frac{\sqrt{5}}{2}$, we take the perturbation $\delta(x) = 0.3\,\delta_0(0.15\,x)$ with

$$\delta_0(x) = \begin{cases} -K + (1+K)|x| & \text{if } |x| < 1, \\ 2 - |x| & \text{if } 1 \leq |x| < 2, \\ 0 & \text{otherwise.} \end{cases} \tag{7.3}$$

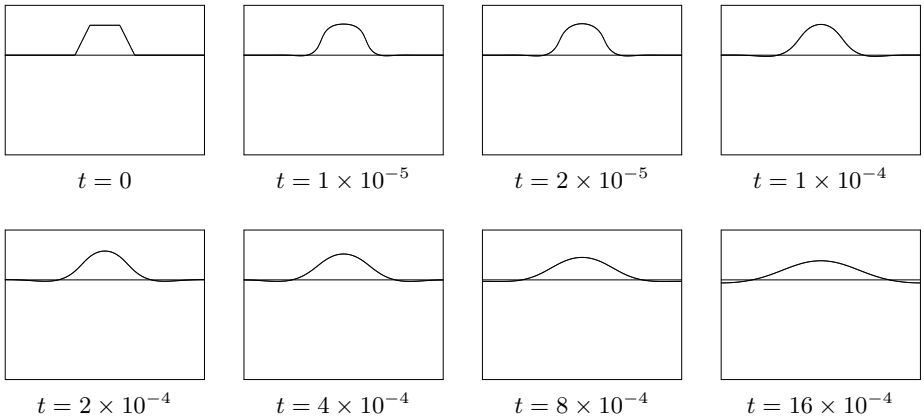

FIG. 7.2. *Solutions for $f \equiv 0$ and $u_0(x) = 1 + \delta(x)$, with $\delta(x)$ a positive perturbation at various times t. In all the plots, the x-axis ranges from -1 to 1, and the y-axis ranges from 0 to 1.5.*

δ is steep and its meanvalue vanishes (see Figure 7.3). We compute the approximate solution with linear elements, and parameters $h = 1/128$, $\tau = 10^{-7}$. The most

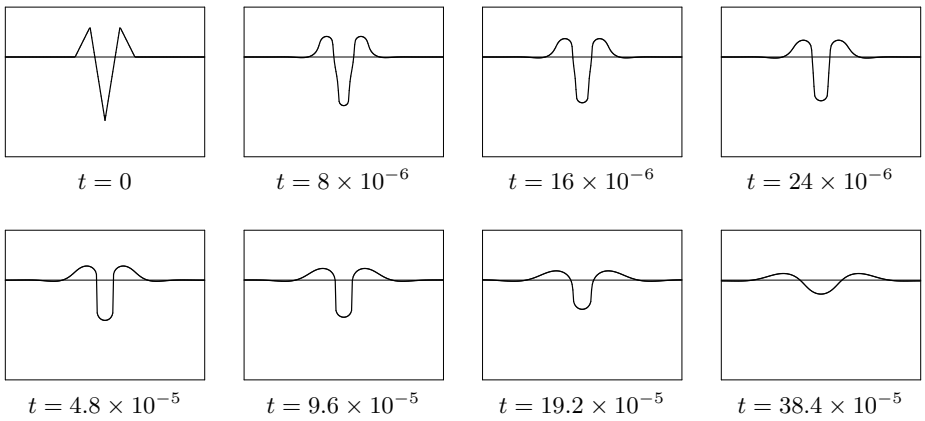

FIG. 7.3. *Solutions for $f \equiv 0$ and $u_0(x) = 1 + \delta(x)$ at various times t, with a steep perturbation $\delta(x)$. In all the plots, the x-axis ranges from -1 to 1, and the y-axis ranges from 0 to 1.5.*

important features of δ are its steep slope together with a big jump of 1st derivative around $x = 0$. As can be seen in Figure 7.3, the slope seems to become vertical around $t = 4.8 \times 10^{-5}$, which indicates that the classical solution might cease to exist in finite time; in contrast the *discrete* solution exists globally in time (see Section 3). We stress that the lack of smoothness of u_0 plays a secondary role since starting with the (smooth) solution $u(t)$ for some small $t > 0$ would yield the same evolution.

To investigate the formation of singularities in finite time, we use the parametric formulation of [3, 4] with the same initial data; for more examples and details about the discretization for parametric surfaces we refer the reader to [3, 4]. Since the parametric formulation works for *closed* curves and surfaces, we thus embed the graph of u_0 into a closed curve (see Figure 7.4 top left). For the time scale of Figure 7.3, the effect of this extension is negligible. Figure 7.4 displays a sequence of solutions obtained for the same eight time instants of Figure 7.3. We see that the parametric

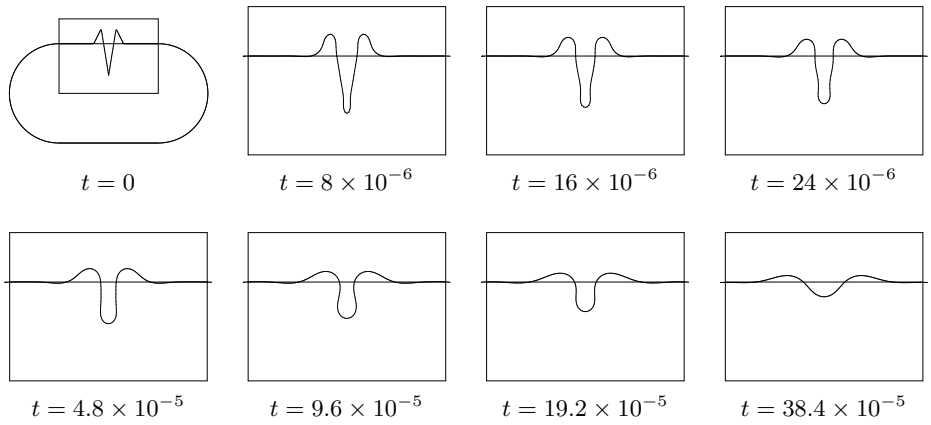

FIG. 7.4. *Solutions obtained with a discretization for parametric curves from [3, 4] at the same times of Figure 7.3. In all the plots, the rectangles in thin lines are* $[-1,1] \times [0,1.5]$.

evolution by surface diffusion tends to form a *mushroom* starting with this initial condition. Therefore, we conclude that the *continuous* solution will cease to be the graph of a function in finite time, i.e., the exact solution to the graph formulation of surface diffusion exists only *locally* in time for certain initial conditions. To assess the range of validity of the graph formulation, namely to be able to detect blow-up, time and space adaptivity might be relevant. It is worth noticing the striking similarity of the solutions obtained with both methods. Even though the parametric solution develops a mushroom at $t = 9.6 \times 10^{-5}$, and thus the solution to the graph formulation is questionable thereon, they still exhibit an excellent quantitative agreement for $t > 9.6 \times 10^{-5}$ (compare the last two plots of Figures 7.4 and 7.3).

7.4. Smoothing Effect in 2d: Case $f \equiv 0$. In this section we present experimental results in $\Omega = (-1,1) \times (-1,1)$ concerning the behavior of the discrete solution when $f \equiv 0$ and $u_0(x) = 1 + \delta(x)$ is a perturbation of the solution $u \equiv 1$.

Positive Perturbation. We consider a positive perturbation as depicted in Figure 7.5, and compute the approximate solution with linear elements and parameters $h = 1/16$, $\tau = 10^{-6}$. Figure 7.5 displays the solution for different time instants. We

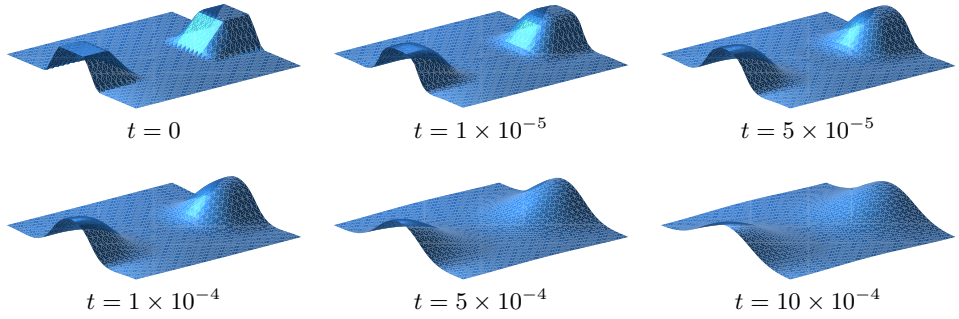

FIG. 7.5. *Solutions for* $f \equiv 0$ *and* $u_0(x) = 1 + \delta(x)$ *at various time instants, with* $\delta(x)$ *a positive perturbation touching the periodic boundary.*

observe, as in the 1d case, a strong smoothing effect much faster for high frequencies than for low frequencies, as well as the solution becoming less than 1 (lack of

maximum principle).

7.5. Crack Formation in 1d: Case $f = -C/u$. We study here the effect of a prescribed forcing of the form $f = -C/u$, which is motivated by the following stationary situation in 1d and corresponding linearized stability analysis.

Equilibrium Shape of Deformable Solids. Following [5], we consider a 2d thin solid occupying the domain $\{(x, y) : -1 \le x \le 1\,,\ 0 \le y \le u(x)\}$ and undergoing a plastic deformation due to competition of elastic effects and surface tension with volume constraint $\int_{-1}^{1} u = 2$. The solid is to adjust its shape in order to minimize the following energy:

$$\mathcal{I}(u, v, \lambda) := \int_{-1}^{1} \sqrt{1 + |u_x|^2} + \frac{1}{2} \int_{-1}^{1} u|v_x|^2 - \lambda\Big(\int_{-1}^{1} u - 2\Big). \tag{7.4}$$

where $u(x)$ describes the free surface of the film, $v(x)$ is the displacement of the solid, and λ is a Lagrange multiplier associated with the volume constraint. Hence, the first term in (7.4) corresponds to surface tension whereas the second one is the elastic energy provided the displacement v solely depends on the horizontal variable x. Upon variational differentiation with respect to u, v and λ, the Euler-Lagrange equations turn out to be

$$-\Big(\frac{u_x}{\sqrt{1 + |u_x|^2}}\Big)_x + \frac{1}{2}|v_x|^2 - \lambda = 0, \qquad (uv_x)_x = 0 \qquad \int_{-1}^{1} u = 2.$$

This immediately yields $v_x = \frac{C}{u}$, whence the equation for u reads

$$-\Big(\frac{u_x}{\sqrt{1 + |u_x|^2}}\Big)_x + \frac{C}{u^2} - \lambda = 0.$$

Linearized Stability Analysis. Since $u \equiv 1$ is a solution of (1.1), then a perturbation w of u evolves for short time according to the linearized PDE around u:

$$\partial_t w = -\Delta(\Delta w + f'(u)w),$$

where $f(u) = -C/u^\gamma$ from the previous discussion, with $\gamma > 0$. Taking an ansatz $w = e^{\mu t} e^{i\pi k x}$ periodic in $(-1, 1)$, we obtain the spectral relation

$$\mu = -(\pi k)^4 + C\gamma(\pi k)^2. \tag{7.5}$$

This implies that $\mu > 0$ provided $(\pi k)^2 < C\gamma$, whence low frequency perturbations grow and the rest decay for short time (*linear regime*).

In the simulations below, we make the simplest choice $\gamma = 1$ and take $C = 50$. Our goal is to explore the long time behavior of (1.1) not predicted by (7.5) (*nonlinear regime*). We discretize the nonlinear forcing term $f(u)$ explicitly, namely $f_{n+1} = -I_h(C/u_h^n)$, and use linear finite elements with parameters $h = 1/128$, $\tau = 10^{-5}$.

Superposition of Sines. We consider the sinusoidal perturbation of (7.1). Figure 7.6 displays the solution at different time instants and shows that high frequencies are rapidly damped whereas the low frequencies slowly lead to a crack formation. This is consistent with the linearized stability analysis (7.5) according to which the frequency $k = 1$ is the only unstable mode.

Positive Perturbation. We consider the perturbation δ of (7.2) and display the results in Figure 7.7, which shows an evolution towards crack formation in finite time.

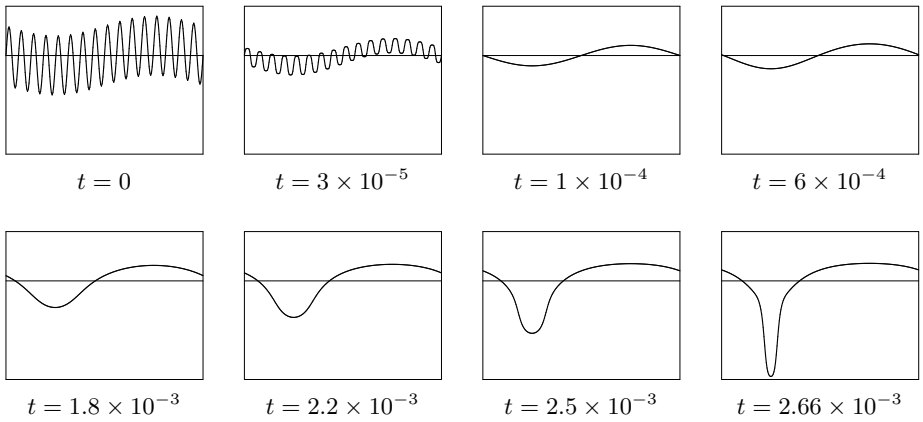

FIG. 7.6. *Solutions for* $f = -50/u$ *and* $u_0(x) = 1 + 0.1\sin(\pi x) + 0.3\sin(16\pi x)$ *various time instants. In all the plots, the* x*-axis ranges from* -1 *to* 1*, and the* y*-axis ranges from* 0 *to* 1.5*.*

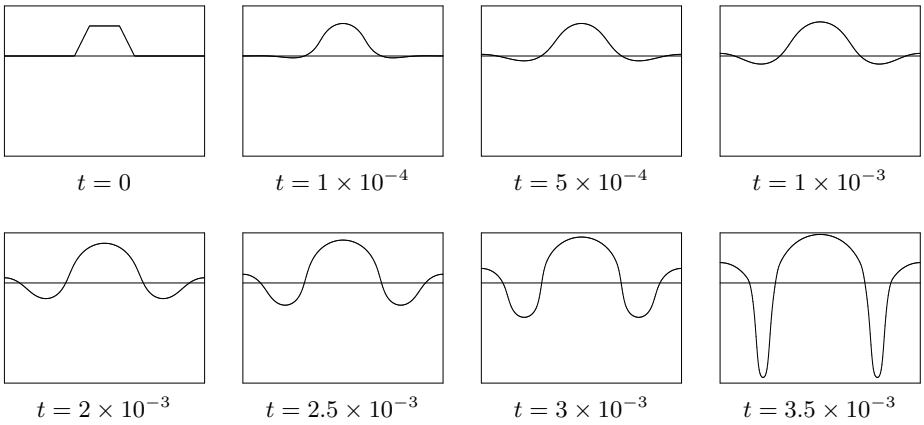

FIG. 7.7. *Solutions for* $f = -50/u$ *and* $u_0(x) = 1 + \delta(x)$ *at various time instants, with* $\delta(x)$ *the positive perturbation of* (7.2)*. In all the plots, the* x*-axis ranges from* -1 *to* 1*, and the* y*-axis ranges from* 0 *to* 1.5*.*

Small Perturbation. We consider a perturbation $\delta(x) = 0.1\,\delta_0(0.02\,x)$ with δ_0 given in (7.3). Simulations are depicted in Figure 7.8, which shows that by $t = 2\times10^{-5}$ the solution is smoothed out. It seems that we have reached a constant equilibrium for a relative long time $t \cong 7.5 \times 10^{-3}$ (*metastable state*). Then an instability grows and a fracture starts to form. The latter develops rather fast.

In order to shed light on the actual evolution during the transition between the fast smoothing of the perturbation and the crack development, we show in Figure 7.9 the solution at some time instants between 2×10^{-5} and 7.5×10^{-3}, with the y axis ranging between 0.998 and 1.001. Even though $u(t)$ looks constant to the eye in Figure 7.8 for t in this interval, a magnification of the y axis shows that this is not the case: some long waves survive the smoothing effect, and at some point they start to increase.

Figure 7.10 displays the Fourier modes of $u(t)$ at times $t = 0, 10^{-5}, 10^{-2}, 3\times10^{-2}$. We observe that all the modes except the first two decrease immediately, whereas the first two modes increase. This is consistent with the prediction (7.5) of linearized

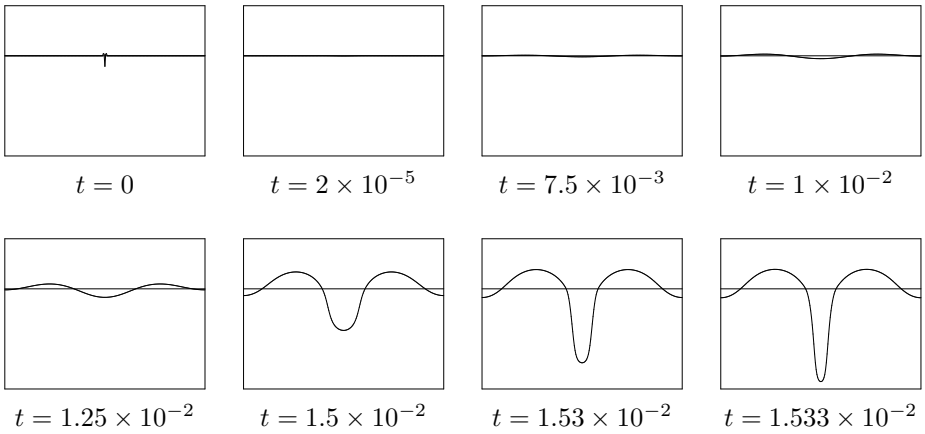

FIG. 7.8. *Solutions for $f = -50/u$ and $u_0(x) = 1 + \delta(x)$ at various times instants, with $\delta(x)$ a small Lipschitz perturbation. In all the plots, the x-axis ranges from -1 to 1, and the y-axis ranges from 0 to 1.5.*

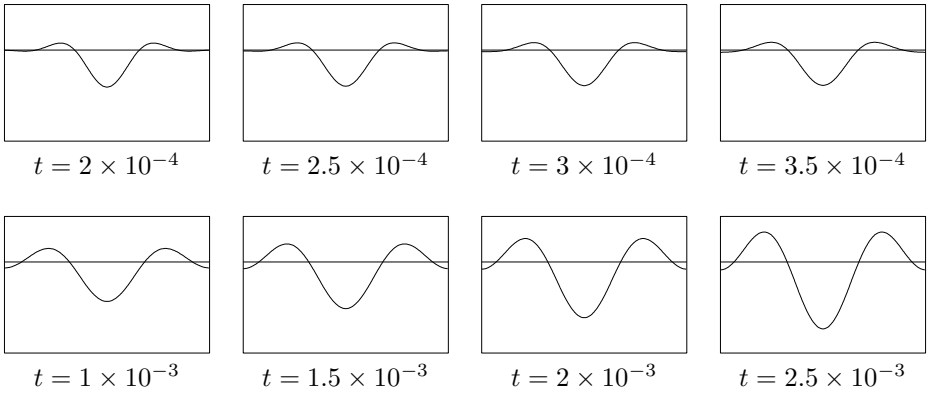

FIG. 7.9. *Solutions for $f = -50/u$ and $u_0(x) = 1 + \delta(x)$ at various time instants between $t = 2 \times 10^{-5}$ and $t = 7.5 \times 10^{-3}$, with the small perturbation of Figure 7.8. In all the plots, the x-axis ranges from -1 to 1, and the y-axis ranges from 0.998 to 1.001.*

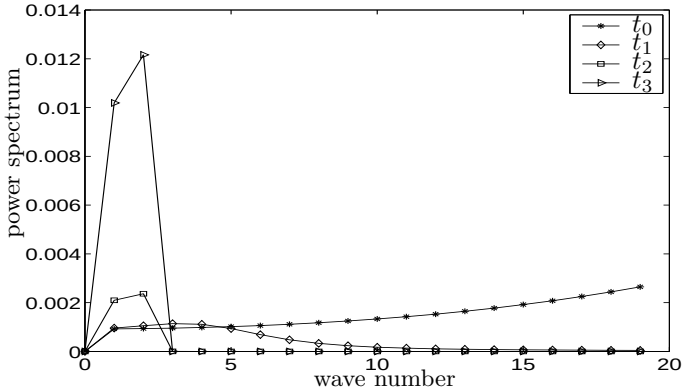

FIG. 7.10. *Power spectrum for the solutions with $f = -50/u$ and $u_0(x) = 1 + \delta(x)$, with the perturbation δ of Figure 7.8. The time instants are $t_0 = 0$, $t_1 = 10^{-5}$, $t_2 = 10^{-2}$ and $t_3 = 3 \times 10^{-2}$.*

stability because $k^2\pi^2 < 50$ implies $k \leq 2$.

Other simulations, also with forcing $f = -50/u$, do not corroborate this apparent consistency with the linearized stability analysis. We observe that, for a fixed *high* frequency, the solution either develops a crack or tends to the steady solution $u = 1$ depending on the *size* of the perturbation; for instance, if $u_0(x) = 1+\alpha \sin(4\pi x)$, then a crack forms for $\alpha \geq 0.2375$ thus violating the prediction $k^2\pi^2 < 50$ of (7.5). On the other hand, for a low frequency, the solution always develops a crack regardless of the perturbation magnitude; for instance, if $u_0(x) = 1 + \alpha \sin(1\pi x)$ a crack forms for all $0.001 \leq \alpha \leq 0.5$ tested. These simulations will be reported elsewhere. We also refer to [8, 10], where simulations under axial symmetry, but without forcing, are performed and singularities are observed as well, which do not conform to the linearized stability analysis either.

7.6. Crack Formation in 2d: Case $f = -C/u$. We conclude this section with the evolution of 2d surfaces immersed in $\mathbb{R}^3$. We consider again the initial surface to be $u_0 = 1 + \delta$, where δ is a perturbation similar to that of Figure 7.3. First we choose such δ across the periodic curve $y = \cos x$ (see Figure 7.11), and finally across the circle $x^2 + y^2 = 1/4$ centered at the origin (see Figure 7.12). We compute with linear elements and parameters $h = 1/16$, $\tau = 10^{-6}$. We observe first

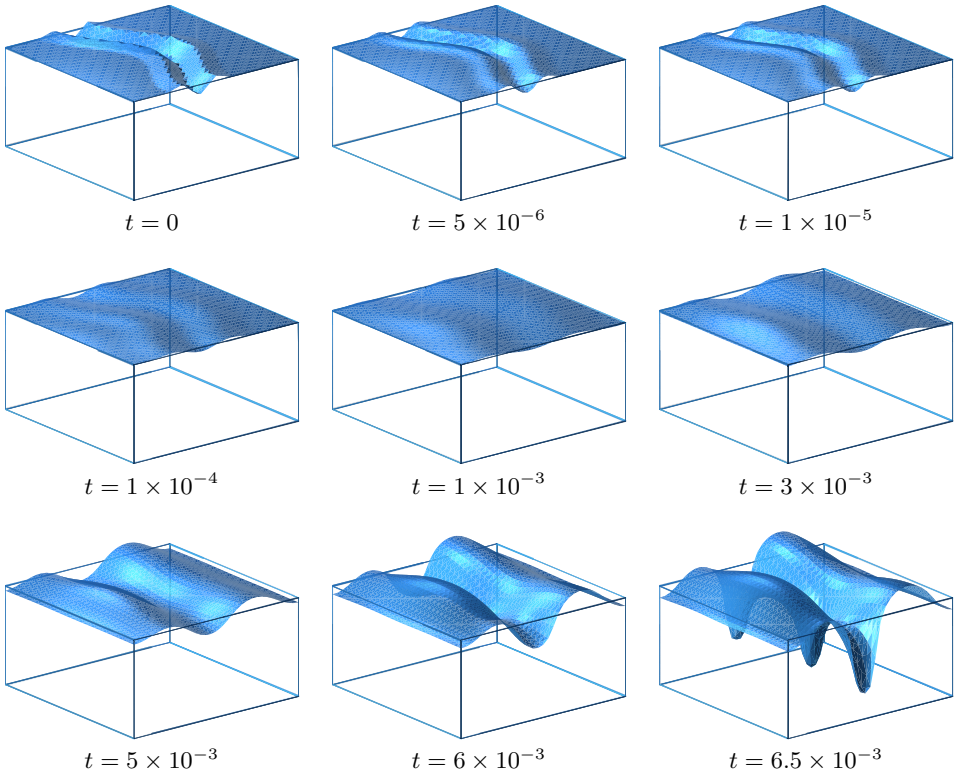

FIG. 7.11. *Solutions for $f = -50/u$ and $u_0(x) = 1 + \delta(x)$ at various time instants, with $\delta(x)$ a small perturbation across $y = \cos x$.*

a smoothing effect followed by crack formation. The latter seems to occur at isolated points rather than lines as illustrated in Figures 7.11 and 7.12. This happens even for 1d profiles in 2d: point singularities seem to be preferred by this evolution.

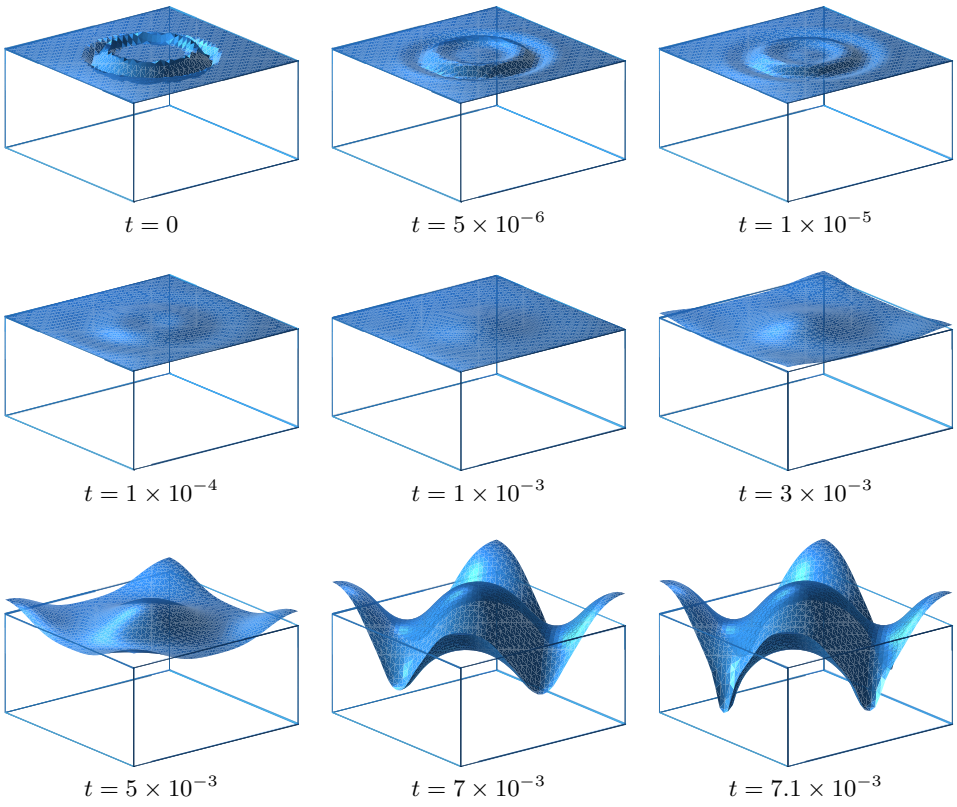

FIG. 7.12. *Solutions for* $f = -50/u$ *and* $u_0(x) = 1 + \delta(x)$ *at various time instants, with* $\delta(x)$ *a small perturbation across* $x^2 + y^2 = 1/4$.

Acknowledgments. We would like to thank J. Collin and M. Grinfeld who originated our interest in surface diffusion. We were all partially supported by the international cooperation NSF-DAAD Grants INT-9910086 and INT-0129243.

REFERENCES

[1] R. J. Asaro and W. A. Tiller, *Surface morphology development during stress corrosion cracking: Part I: via surface diffusion*, Metall. Trans., 3 (1972), pp. 1789-1796.
[2] E. Bänsch, *Local Mesh Refinement in 2 and 3 Dimensions*, IMPACT of Computing in Science and Engineering, 3 (1991), pp. 181–191
[3] E. Bänsch, P. Morin, and R.H. Nochetto, *Finite element methods for surface diffusion*, Proceedings of Free Boundary Problems: Theory and Applications, Trento, 2002 (to appear).
[4] E. Bänsch, P. Morin, and R.H. Nochetto, *A finite element method for surface diffusion: The parametric case*, (to appear).
[5] E. Bonnetier, R. Falk, and M. Grinfeld, *Analysis of a one-dimensional variational model of the equilibrium shape of a deformable crystal*, M2AN Math. Model. Numer. Anal., 33 (1999), pp. 573–591.
[6] S.C. Brenner, L.R. Scott, *The Mathematical Theory of Finite Element Methods*, Springer-Verlag 2002.
[7] J. Cahn and J. Taylor, *Surface motion by surface diffusion*, Acta Metall. Mater., 42 (1994), pp. 1045–1063.
[8] B. Coleman, R. Falk, and M. Moakher, *Space-time finite element methods for surface diffusion with applications to the theory of the stability of cylinders*, SIAM J. Sci. Comput., 17 (1996), pp. 1434–1448.

[9] K. Deckelnick and G. Dziuk *Error estimates for a semi-implicit fully discrete finite element scheme for the mean curvature flow of graphs,* Interfaces and Free Bound., 2 (2000), pp. 341–359.

[10] K. Deckelnick, G. Dziuk, and C.M. Elliott, *Error analysis of a semidiscrete numerical scheme for diffusion in axially symmetric surfaces*, (to appear).

[11] G. Dziuk, *Numerical schemes for the mean curvature flow of graphs,* Variations of domain and free-boundary problems in solid mechanics (Paris, 1997), pp. 63–70, Solid Mech. Appl., 66, Kluwer Acad. Publ., Dordrecht (1999).

[12] M.A. Grinfeld, *Thermodynamic Methods in the Theory of Heterogeneous Systems*, Longman, New York, 1991.

[13] C. Herring, *Surface tension as a motivation for sintering*, in The Physics of Powder Metallurgy, Editor: W. E. Kingston, McGraw-Hill, New York, pp. 143-179, 1951.

[14] W.W. Mullins, *Theory of thermal grooving*, J. Appl. Phys., 28 (1957), pp. 333.

[15] A. Schmidt and K.G. Siebert, *ALBERT: An adaptive hierarchical finite element toolbox*, Documentation, Preprint 06/2000 Universität Freiburg, 244 p.

[16] A. Schmidt and K.G. Siebert, *ALBERT — Software for Scientific Computations and Applications*, Acta Math. Univ. Comenianae 70 (2001), pp. 105–122.

[17] B.J. Spencer, S.H. Davis, and P.W. Voorhees, *Morphological instability in epitaxially-strained dislocation-free solid films: nonlinear evolution*, Phys. Rev. B, 47 (1993), pp. 9760-9777.

[18] B.J. Spencer and D.I. Meiron, *Nonlinear evolution of the stress-driven morphological instability in a two-dimensional semi-infinite solid*, Acta Metall. Mater. Vol., 42 (1994), pp. 3629-3641.

[19] D.J. Srolovitz, *On the stability of surfaces of stressed solids*, Acta metall., 37, (1989), pp. 621-625.